AD-A153 967 TARGET IDENTIFICATION USING GLOBAL AND LOCAL FEATURES (U) ARIZONA UNIV TUCSON ENGINEERING EXPERIMENT STATION D G DUDLEY 11 MAR 85 N00019-83-C-0362 1/1

UNCLASSIFIED F/G 20/6 NL

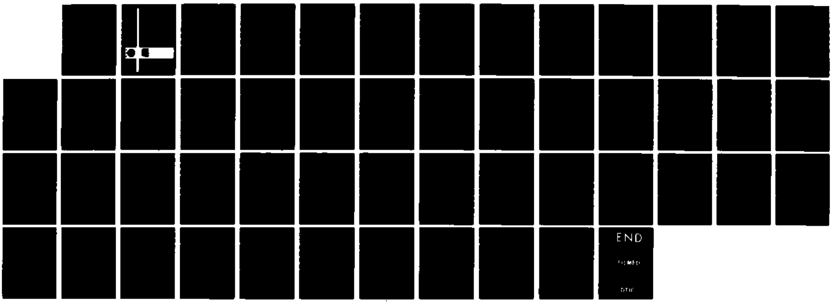

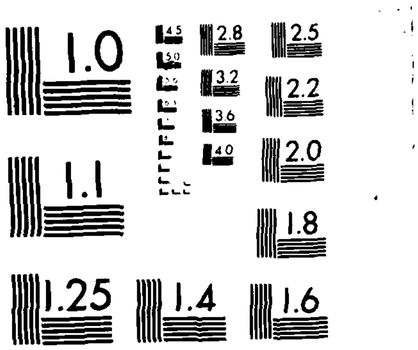

MICROCOPY RESOLUTION TEST CHART
NATIONAL BUREAU OF STANDARDS 1963-A

AD-A153 967

(2)

FINAL REPORT

Contract No. N00019-83-C-0362

TARGET IDENTIFICATION USING GLOBAL AND LOCAL FEATURES

Submitted by:

D.G. Dudley

Submitted to:

Naval Air Systems Command
Department of the Navy
Naval Air Systems Command Headquarters
Washington, D.C. 20361

ENGINEERING EXPERIMENT STATION
COLLEGE OF ENGINEERING
THE UNIVERSITY OF ARIZONA
TUCSON, ARIZONA

SECURITY CLASSIFICATION OF THIS PAGE

REPORT DOCUMENTATION PAGE

1a. REPORT SECURITY CLASSIFICATION: Unclassified

1b. RESTRICTIVE MARKINGS:

2a. SECURITY CLASSIFICATION AUTHORITY:

2b. DECLASSIFICATION/DOWNGRADING SCHEDULE:

3. DISTRIBUTION/AVAILABILITY OF REPORT: Approved for public release; distribution unlimited.

4. PERFORMING ORGANIZATION REPORT NUMBER(S):

5. MONITORING ORGANIZATION REPORT NUMBER(S):

6a. NAME OF PERFORMING ORGANIZATION: Engineering Experiment Station, College of Engineering

6b. OFFICE SYMBOL *(If applicable)*:

7a. NAME OF MONITORING ORGANIZATION: Naval Air Systems Command, Department of the Navy

6c. ADDRESS *(City, State and ZIP Code)*:
University of Arizona
Tucson, AZ 85721

7b. ADDRESS *(City, State and ZIP Code)*:
Air-330R
Naval Air Systems Command Headquarters
Washington, D.C. 20361

8a. NAME OF FUNDING/SPONSORING ORGANIZATION:

8b. OFFICE SYMBOL *(If applicable)*:

9. PROCUREMENT INSTRUMENT IDENTIFICATION NUMBER: N00019-83-C-0362

8c. ADDRESS *(City, State and ZIP Code)*:

10. SOURCE OF FUNDING NOS.

PROGRAM ELEMENT NO.	PROJECT NO.	TASK NO.	WORK UNIT NO.

11. TITLE *(Include Security Classification)*: Target Identification Using Global and Local Features

12. PERSONAL AUTHOR(S): Dudley, Donald G.

13a. TYPE OF REPORT	13b. TIME COVERED	14. DATE OF REPORT (Yr., Mo., Day)	15. PAGE COUNT
Final Report	FROM 9/23/83 TO 3/23/85	March 11, 1985	50

16. SUPPLEMENTARY NOTATION: The findings of this report are not to be construed as an official Department of the Navy position, unless so designated by other authorized documents.

17. COSATI CODES

FIELD	GROUP	SUB. GR.

18. SUBJECT TERMS *(Continue on reverse if necessary and identify by block number)*: Target identification, target classification, system identification, parametric modeling, pole-zero modeling, complex resonance identification.

19. ABSTRACT *(Continue on reverse if necessary and identify by block number)*

This report is concerned with input-output data from an electromagnetic process. The input is a component of the field generated by the experimenter. The output is a component of the field scattered by an object. The goal is to determine, from the data, characteristics of the scatterer.

We consider both complex exponential (global) and ray-optic (local) modeling. We report results from both simulated data and experimental data obtained on the transient ranges at NOSC and Lawrence Livermore National Laboratory.

In complex exponential modeling, we conclude that pole identification can be accomplished to a high degree of accuracy. Relating these data poles to complex resonances of the scatterer, however, is limited to high-Q cases in a low noise environment.

Our results in ray-optic modeling are preliminary. We find serious difficulties

20. DISTRIBUTION/AVAILABILITY OF ABSTRACT: UNCLASSIFIED/UNLIMITED ☒ SAME AS RPT. ☐ DTIC USERS ☐

21. ABSTRACT SECURITY CLASSIFICATION: Unclassified

22a. NAME OF RESPONSIBLE INDIVIDUAL: James Willis

22b. TELEPHONE NUMBER *(Include Area Code)*: 202-692-2510

22c. OFFICE SYMBOL:

DD FORM 1473, 83 APR — EDITION OF 1 JAN 73 IS OBSOLETE.

SECURITY CLASSIFICATION OF THIS PAGE

19.

in discriminating between smooth objects with the same radius of curvature and between identifical objects with different curvatures.

TABLE OF CONTENTS

LIST OF ILLUSTRATIONS

LIST OF ILLUSTRATIONS -- Continued

1. INTRODUCTION

In this report, we are concerned with input-output data associated with a transient electromagnetic process. The input is defined as a component of the electromagnetic field generated by the experimenter. An example is the vertical electric field at point P in the absence of a scattering object. The output is defined as a component of the electromagnetic field scattered by the scattering object. An example is the vertical electric field at the same point P obtained in the presence of the scatterer by subtracting the total field from the incident field. The goal of the electromagnetic experiment is, given the input-output data, determine characteristics of the scattering object.

In a previous report (Dudley, 1984a), we considered parametric models. We defined models whose parameters can be varied so as to make the output from the model "close" in some sense to the output from the actual electromagnetic experiment. This procedure is called the "system identification problem." Following the identification, we considered the possibility of determining physical characteristics of the electromagnetic process from the parameters identified during the identification process. This procedure is called the "classification problem."

The results reported in Dudley (1984a) were based principally on complex resonance identification techniques. Through use of the non-linear least squares algorithm NLS (Goodman, 1983), successful identification and classification procedures were carried out on simulated data obtained from solving forward problems associated with several canonical structures. Difficulties arose, however, in making the transition from identification to classification except under the following restrictions. First, the complex resonances must contain only small damping. Second, the resonances must be distinctly separated. Third, the signal-to-noise ratio must be high.

In order to appreciate the significance of these limitations to complex resonance modeling, it is crucial to understand the distinction between identification and classification. Using the NLS algorithm on simulated data, we have been able to match the output from our model to the output from the electromagnetic process, usually to within better than one part in 10^{-4}. The poles thus obtained are accurate poles of the data. Their physical significance, however, is another matter. Our conclusions have been that there is little chance of relating the data poles to the natural resonances of the object except under the above three restrictions.

In addition to the three restrictions mentioned above, Dudley (1984a) has discussed the fact that there is more information available in the transient wave than that contained in the complex resonance model. Indeed, for perfectly conducting scatterers, it has been shown (Marin, 1973; Pearson, 1984; Morgan, 1984) that the scattering consists, in the complex frequency domain, of a series over complex poles plus an entire function. The inverse Laplace transform yields a complex exponential series, arising from the pole series, plus an additional term, arising from the entire function. As discussed by Dudley (1985), the complex exponential series is parametrized by the complex poles and residues, but the entire function is not parametrized at all. The complex exponential model does not contain the entire function term and thereby treats it as noise in the noise minimization process leading to the identification of the coefficients in the complex exponential series. This is unfortunate, because there is information available in the entire function that is being ignored.

There has been some discussion during meetings of the International Union of Radio Science concerning the possibilities of utilizing the time-limited characteristic of the entire function (Morgan, 1984) to determine a point in the time signature beyond which a pure complex exponential model is appropriate. We shall consider the merits of this point of view subsequently.

In this report, we continue with our studies of complex exponential modeling. We report further studies with simulated data and follow with results with actual data, obtained on the NOSC and Lawrence Livermore National Laboratory (LLNL) transient ranges. In order to begin to understand information not utilized in the complex exponential model, we describe some experimental models constructed to study local feature scattering. We show some preliminary results from scattering experiments on these models performed at NOSC. The report concludes with a discussion of results and some recommendations for further research.

2. COMPLEX RESONANCE IDENTIFICATION

In this section, we begin by describing results with simulated data obtain from scattering from a hard acoustic sphere. We include these results to dramatize difficulties with objects displaying large radiation damping. We next describe backscatter experiments on aluminum plates, experiments performed at both NOSC and LLNL. We conclude the section with some definitive statements concerning the future of complex exponential modeling in target identification.

2.1 The Hard Acoustic Sphere, Simulated Data

In our previous report (Dudley, 1984a), we identified the complex resonances from dielectric slabs. We were able to make the bridge between identifying the complex resonances in the data (system identification) and calculation of the thickness and dielectric constant of the slabs (classification), so long as the data was characterized by a high signal-to-noise ratio. The slab problem, however, contained no radiation damping in the scattered field. Such an ideal situation cannot be anticipated in practice. Indeed, the sphere is a canonical example containing severe radiation damping. In addition, the sphere contains an early time contribution, due to the entire function, that is not included in the complex resonance model. We limit ourselves to the acoustic case because it is simpler and yet still provides the insight we seek.

Consider acoustical backscatter from a hard sphere (Neumann boundary conditions). We solve this problem in the frequency domain by summing the well-known Mie-series (Bowman, et. al., 1969). We next multiply the solution by the spectrum of the incident pulse and take the inverse Fourier transform numerically by Filon's method (Dudley, 1975). We use the input-output time-domain data so obtained as simulated data for the NLS algorithm.

Consider the specific case of backscatter from a sphere of radius 1 meter with observation point at 10 meters. The input signal (Fig. 1) is selected to give a bandpass characteristic in the frequency domain (Fig. 2). Its selection is part of an ongoing effort to shape the input spectrum to the identification problem at hand. The reponse to this input at r = 10 meters (Fig. 3) is characterized by an initial response, followed by the first creeping wave. By the time the second creeping wave is due, the radiation damping has eliminated its appearance in the waveform. The Fourier transform of the output signal (Fig. 4) exhibits several resonances that we shall attempt to identify. We low-pass filter the data at 300 hertz and then decimate to avoid oversampling. The resulting input (Fig. 5) and output (Fig. 6) consist of 200 sample points. We next do an identification of the complex resonances using the NLS algorithm.

The location of the identified poles (x) in the complex s-plane are displayed (Fig. 7) for a 17th order model, along with the theoretical poles (+). The process is repeated (Fig. 8) for a 40th order model. The number of poles within the passband of the filter is approximately 13, with the energy concentrated about 150 hertz. Note that there is little correspondence between the 17th order identified poles and their theoretical counterparts, despite the fact that the model output and the simulated output agree throughout the waveform to one part in 5000. For the 40th order model (Fig. 8), the situation is not much better, despite model and simulated output agreement to one part in 100,000.

It is clear that complex resonance identification has been performed very accurately. That is, there is excellent agreement between the model and simulated output. There is, however, little agreement between the theoretical and identified poles. The classification process has therefore failed. The poles are poles of the data and not poles of the scatterer. We understand why this happens. The fault is not with the algorithm. Indeed, it has produced an excellent match to the data. The fault is in our complex exponential model. The early time return ($0 < t < 0.012$) contains a large contribution from the entire function that is not modeled correctly by our algorithm. In addition, the radiation damping prevents us from observing returns later than the first creeping wave. We therefore are unable to observe multiple returns from successive waves as they circumnavigate the object. If we eliminate the entire function in early time by time windowing, we eliminate all possibility of characterizing body resonances. The reason why this is true is that we destroy the time reference that measures time around the object. If we could observe at least the first and second creeping wave, the time windowing procedure could be attempted. Indeed, such a procedure has been successfully demonstrated for the dielectric slab, where there is no radiation damping. In the case of the sphere, however, the radiation damping drives the second creeping wave and all subsequent ones into the noise. Unfortunately, most targets of interest display large radiation damping effects.

2.2 The Conducting Plate, Transient Range Data

Although we have previously reported plate scattering data taken on the NOSC transient range (Dudley, 1984b), we have since repeated these measurements on the transient range at LLNL. Recent modifications at the LLNL range have dramatically decreased the noise level, to the point where we can obtain more accurate identifications.

The LLNL range (Fig. 9) consists of an IKOR pulser feeding a half-bicone antenna erected on a ground plane. The pulser produces a pulse with less than a .1 nanosecond rise time and a 1 kilovolt peak amplitude. The pulse width is less than 0.15 nanosecond and is transmitted at a 250 hertz repetition rate. Such a pulse has a spectrum flat to within plus or minus 2 db from 1 megahertz to 1 gigahertz. The pulser triggers a Tektronix 7408 Sampling Oscilloscope. The data collected is fed to an LSI-11/23 computer and supplied off-line on floppy discs (RT format) to a VAX11/750. The bicone antenna transmitted signal is received by a d-dot sensor mounted on the ground plane. "Input" data means data taken with the d-dot sensor in the absence of the scattering plate. "Output" data means data taken with the d-dot sensor in the presence of the plate.

Data has been taken and reduced for three rectangular aluminum plates of differing sizes. We shall describe a typical result with a plate 30 centimeters high and 60 centimeters wide. The polarization on the range is vertical. All data taken is backscatter with the d-dot probe located 58.7 inches from the apex of the bicone and the plate located 2 feet behind the d-dot probe. (In Fig. 9, a = 58.7 inches, b = 2 feet.) The experiment has the following objectives:

1. Obtain the natural resonances of the plate
2. Compare the resonances with Pearson (1976)
3. Obtain the transfer function of the plate
4. Compare the transfer function with the Patch Code, which gives a numerical solution.

We shall describe results applicable to the first three objectives. The fourth objective is awaiting results from W. A. Johnson, Sandia National Laboratories. He has been supplied with our data.

The raw input and output data consists of 1024 points with a sampling interval of 1.953×10^{-11} seconds. All waveforms are averaged over 100 shots before recording. Both x-axis and y-axis zero references are set by visual observation of the oscilloscope. Since signals through the d-dot sensor cannot have a dc component, we remove the mean from both the input and output (Fig. 10). Note the low noise level in the input signal. In the output, we comment that our clear time is limited by the artifact return visable at 15.2 nanoseconds. This signal is the scattered pulse from the plate after it has been re-reflected from the apex of the bicone. We next align the input and output and subtract input from output to produce the scattered field (Fig. 11). Note the small residual precursor remaining in the scattered field caused by small difference in successive shots. Since we next front-cut the scattered data, we are in effect ignoring this small error. We next realign the input and output, filter at 2.5 gigahertz and decimate to 128 points (Fig. 12). The resulting input and output spectrum (Fig. 13) appear to have a number of resonances.

We begin the analysis of the preprocessed data by obtaining the bandlimited delta function response (Fig. 14) by Weiner filtering (Dudley, 1983). The impulse response exhibits a number of successive interference-type returns. We attribute these to returns caused by interactions between the plate edges. The bandlimited transfer function is obtained by taking the transform of Figure 14. The result (Fig. 15) shows an increasing amplitude as a function of increasing frequency, plus several resonances. We are awaiting comparison with numerical data from Sandia National Laboratories.

We next process the input-output data (Fig. 12) through the NLS algorithm. We use a 45th order model and obtain a match (Fig. 16) between the model output and the scattered field. Note the relatively high order model necessary in this case. This non-parsimonious model is caused by the necessity of matching a complex exponential series to data that exhibits a burst response followed by relaxation, followed by another burst, and so forth. We compare the first few of our poles (low frequency, low damping) with Pearson (1976). Note (Fig. 17) that for the first two pole pairs there is good agreement in the imagninary parts but poor agreement in the real parts. This result is consistent with known relative sensitivity analyses (Dudley, 1979). We have identified the real frequency of the resonance, but not the damping.

2.3 Conclusions

We have examined in this section and in Dudley (1984a) complex resonance identification with both simulated and experimental data. We find that, though use of an effective signal processing algorithm (SIG) and an interactive non-linear optimizer (NLS), we can perform efficient, accurate identification on a large variety of data. By accurate identification, we mean the adjustment of model parameters such that the output from the model matches the output from the electromagnetic process throughout the range of the signal to within a specified tolerance. Classification is another matter. We find that relating the complex resonances of the data to the natural resonances of the object is an exercise in frustration for all but high-Q resonances in a high signal-to-noise environment.

3. RAY-OPTIC IDENTIFICATION

In this section, we begin by describing experimental models constructed for early time signature tests on the NOSC transient range. We follow with a description of the range. Next, we compare scattering signatures for a variety of cylindrical objects and end by indicating some observations about the future of early time modeling.

3.1 Model Construction

For study on the transient range, we constructed a number of circular and parabolic cylinders. The circular cylinders (Fig. 18) are aluminum tubing. We constructed three models, all 3 feet high. The three have radii of 2, 3, and 4 inches. We also constructed three models with a height of 6 feet and the same radii as above. The parabolic cylinders (Fig. 19) were constructed with aluminum screen stretched over a wooden frame. We constructed two models, both 6 feet high. The first has a radius of curvature of 2 inches; the second, 4 inches. (The radius of curvature of a parabolic cylinder is one half the focal length.) All models were mounted, one at a time, on the NOSC transient range with the cylindrical axis vertical (parallel to the transmitted electric field.)

3.2 The NOSC Transient Range

The transient range at NOSC (Fig. 20) is a bounded wave simulator 45 feet in length. Its principal attribute is its physical size, which makes possible measurements requiring extensive clear time. All of our measurements were performed near the center of the turntable. The results we shall discuss are for backscatter, measured with a d-dot probe of identical design to the probe at the LLNL range.

3.3 Measurements of Cylindrical Structures

Scattering measurements were performed on all models discussed above. Although we have taken and stored a large amount of data, we shall only report results on certain representative members of the total ensemble. We consider backscatter measurements for the following 6-foot high models: The parabolic cylinder with 4 inch radius of curvature (called the 4 inch parabola); the parabolic cylinder with 2 inch radius of curvature; the circular cylinder with 4 inch radius of curvature (called the 4 inch pipe). All scattered data presented is backscatter at 2 feet from the cylinder surface.

As a representative set of the raw data, consider the free field and total field for the 4 inch parabola (Fig. 21). Typically, the scattered field is produced by subtracting the free field from the total field (Fig. 22). Note the precursor caused by shot-to-shot variations. This precursor is more noticable on the NOSC range than the LLNL range and must be considered a source of error in the results. Indeed, we proceed by front-cutting the scattered field data thereby eliminating the precursor.

We next compare the scattered fields from the 4 inch parabola with the 4 inch pipe (Fig. 23). Note the almost perfect match in the time history until the scattering from the back edge of the parabola enters the measurement at 4.7 nanoseconds. We display a similar result for the 4 inch parabola and the 2 inch parabola (Fig. 24). Although, the differences are slightly more pronounced, we still note great difficulty in distinguishing two different objects (parabolic cylinder and circular cylinder) with the same radius of curvature and two objects of the same type (both parabolic cylinders) with different radii of curvature.

3.4 Conclusions

As we begin to investigate early time scattering, we are faced with some serious difficulties, illustrated by the similarities in the scattering signatures of different objects. It is already clear that we must begin to examine object features that are more dramatic than radius of curvature at a single point.

4. DISCUSSION

Our experience with both simulated and transient range data has pointed up some serious limitations in existing methods for parametric classification. We discuss complex resonance methods and ray optic methods and follow with some recommendations.

Over the past decade, there has been a concentrated effort by many researchers to classify with complex resonances. We believe, based on both theory and experimental modeling, that the following definitive statements can be made concerning complex resonance modeling:

(1) Identification with complex resonances can be accomplished with a high degree of accuracy through use of a signal processing algorithm, such as SIG, and an efficient non-linear optimizer, such as NLS. In other words, the output from the parametric model can be adjusted to match the output from the transient electromagnetic process to high accuracy. There is little need for further work in this subject area.

(2) The complex resonances obtained in the procedure in (1) are not guaranteed to bear any resemblance to the natural resonances of the scatterer. There are two difficulties. First, the complex exponential series is a series with very few good mathematical properties. Second, the complex resonance description of the scattered field is

incomplete; the entire function is missing. Our tests show that sucessful transition from poles of the data to poles of the object can only be made in high-Q, low noise situations. These situations rarely occur with objects of practical interest in target identification. We view with extreme pessimism any further attempts to do target natural resonance classification with complex exponential models.

(3) If the entire function is included to make a better model, there is at present no way to parametrize it. The complex exponential series is parametrized by the poles and residues; the entire function is not parametrizeed at all. As matters now stand, the addition of the entire function to the model has only conceptual significance and does not aid in improvement in identification and classification.

(4) Parametrizing the entire function (Dudley, 1985) is the key to further progress in producing a parametric inverse model containing complex resonances. This subject area is an important candidate for continued research.

Studies in ray-optic identification and classification are just beginning. Already, however, we have noted some difficulties. We find that there is very little difference in backscatter signatures from smooth bodies with the same radii of curvature. We also have difficulties with two bodies of identical form but radii of curvature that differ by a factor of 2. These results are expected when one examines the asymptotic series associate with scattering from smooth bodies (Bowman, et. al., 1969).

System identifaction is a well-developed science that has produced many sophisticated algorithms, including one specifically designed for transients (Goodman, 1983). There is little need for electromagnetic researchers in further identification algorithm development. What is needed are better models.

The principal characteristic in transient scattering from targets of interest seems to be successive returns set up by interferences among localized features. These are precisly the features that, when viewed overall, combine to produce the object resonances. Such a combination, however, is often an inefficient descriptor (Felsen, 1985). Our studies with the dielectric slab point out that the local interferences give more efficient information directly in the time domain than their total combination in terms of the complex resonances.

It is recommended that research be directed towards the development of parametric models whose parameters describe both local and global features within a single model structure. Without such a model, a satisfactory parametric inverse method remains elusive.

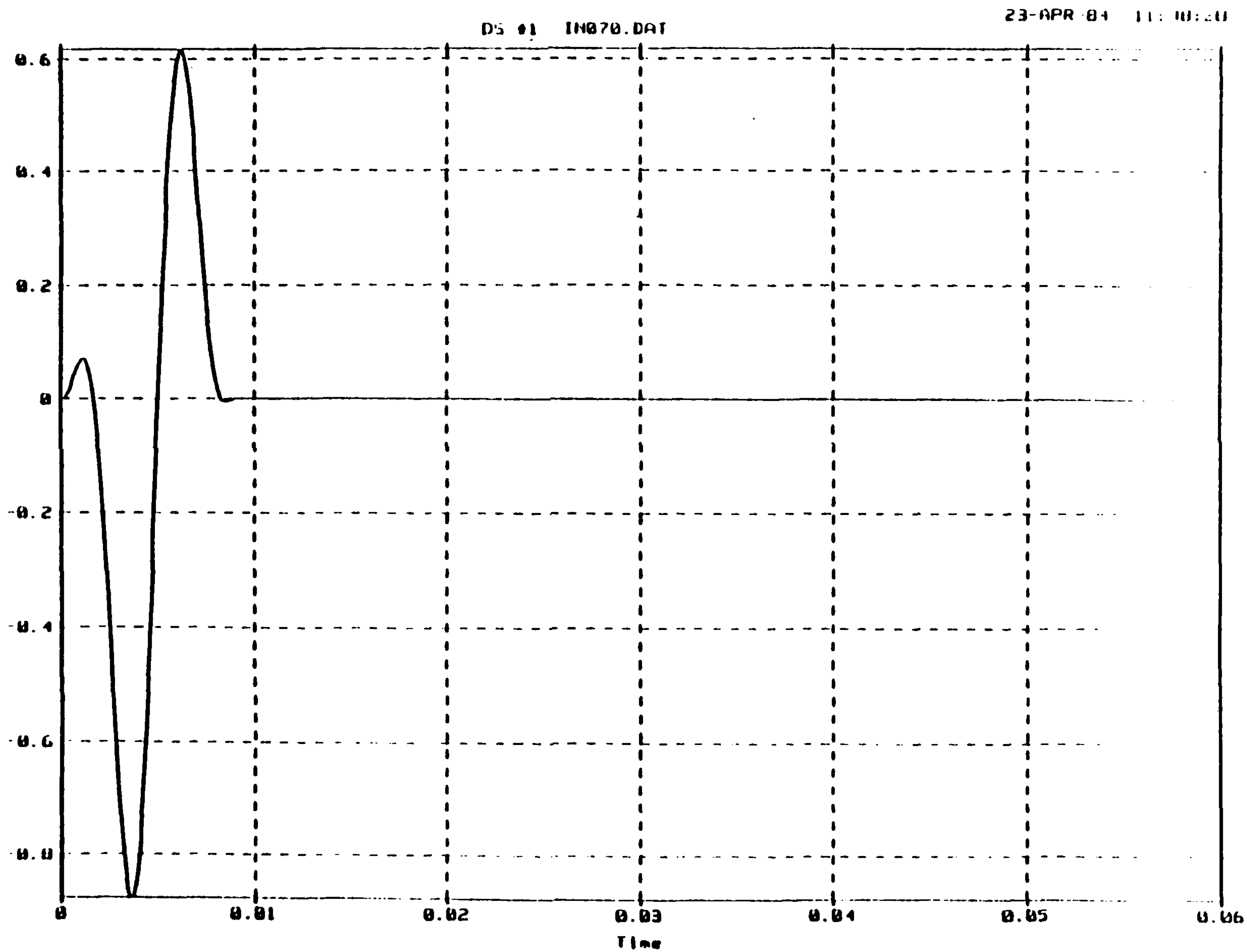

Fig. 1. Input signal, acoustic sphere.

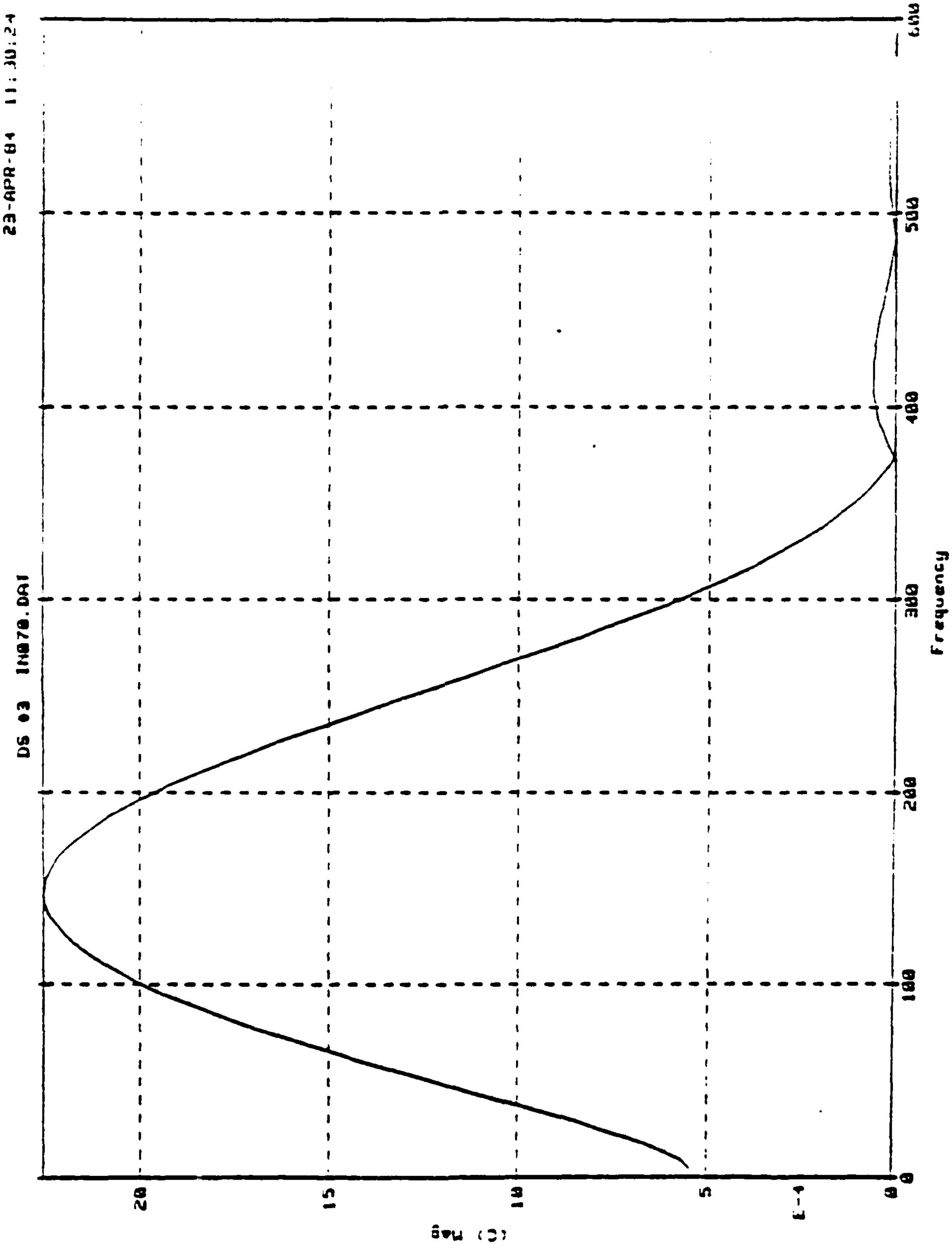

Fig. 2. FFT of input signal.

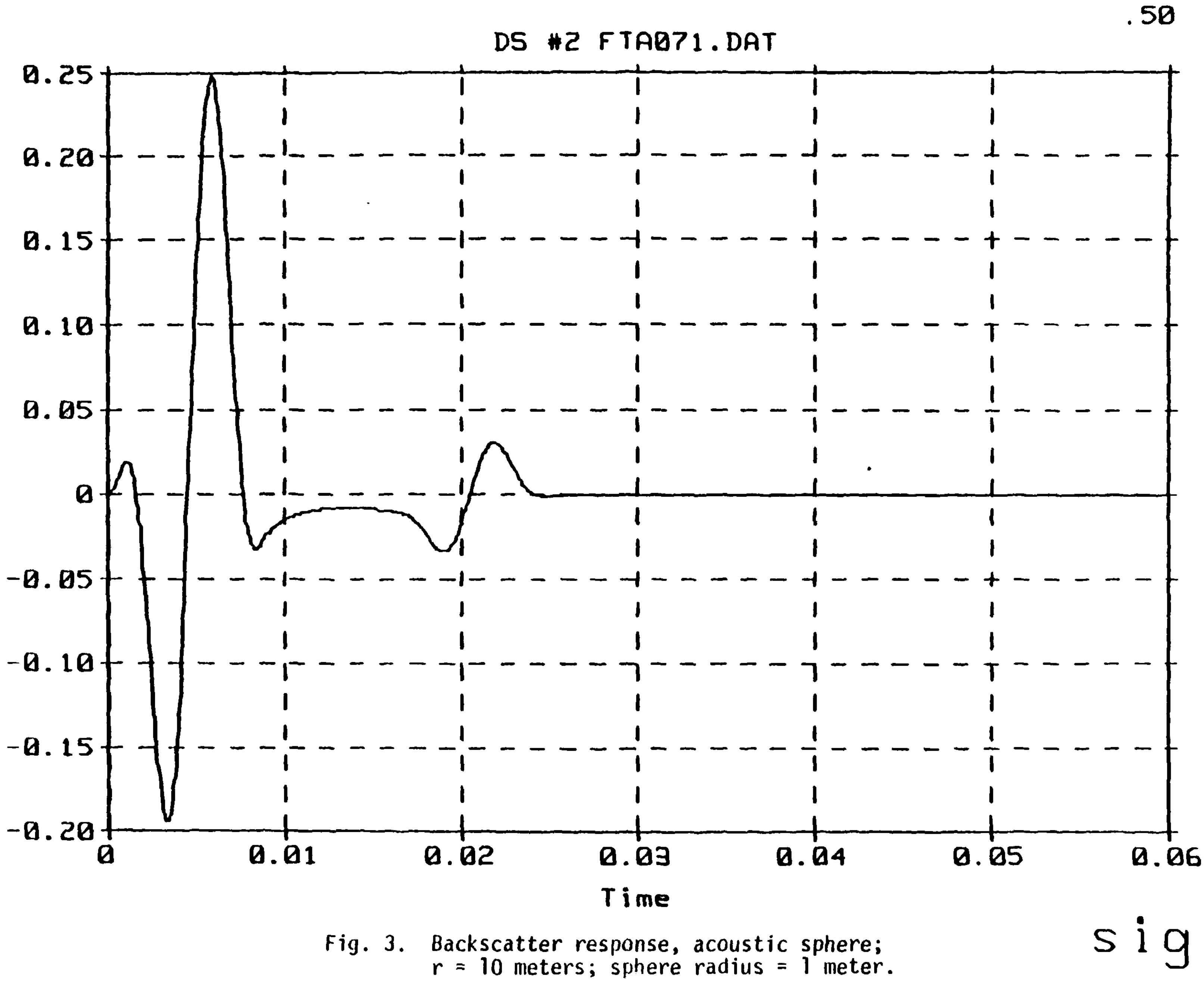

Fig. 3. Backscatter response, acoustic sphere;
r = 10 meters; sphere radius = 1 meter.

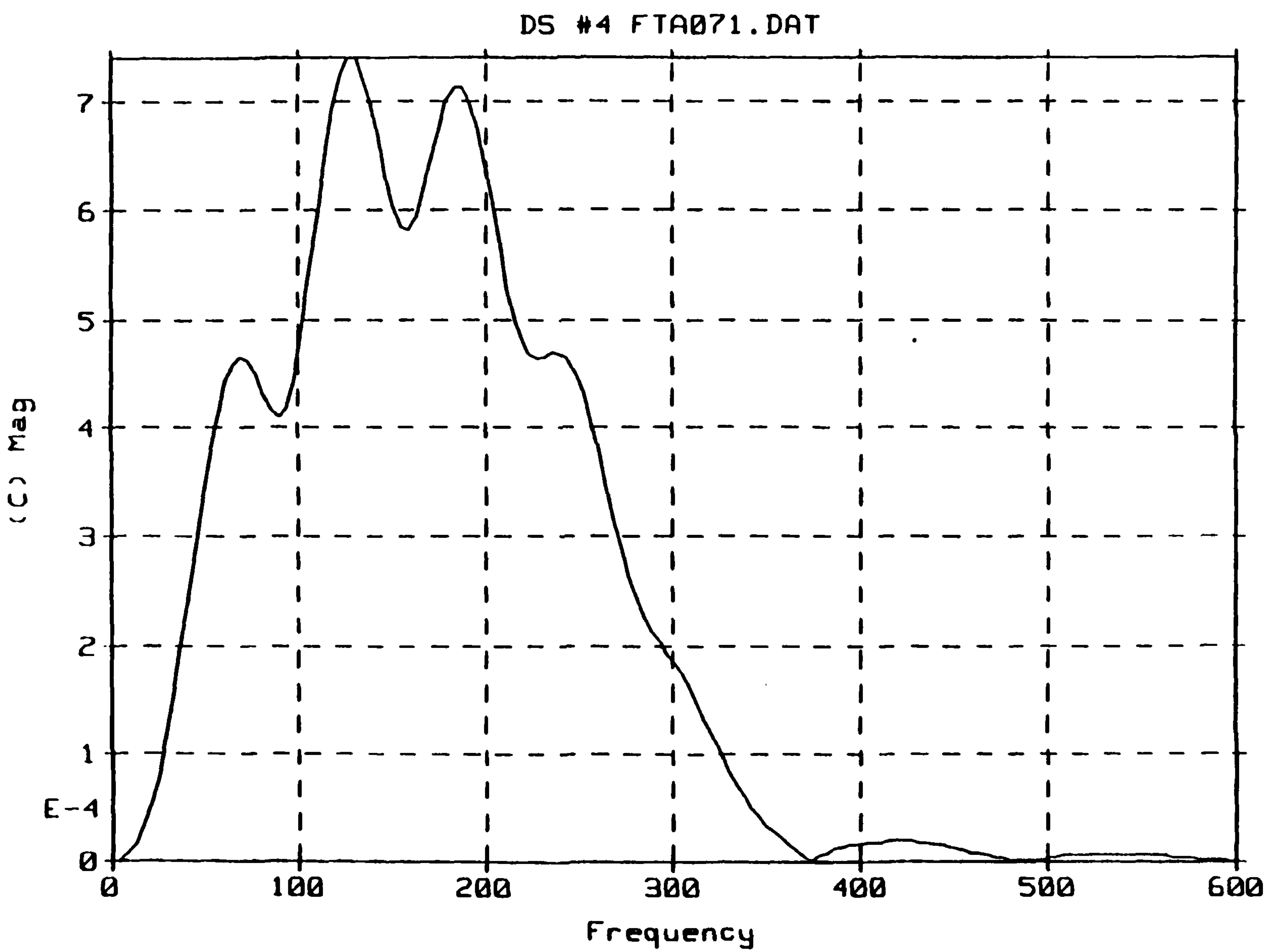

Fig. 4. FFT of backscatter response.

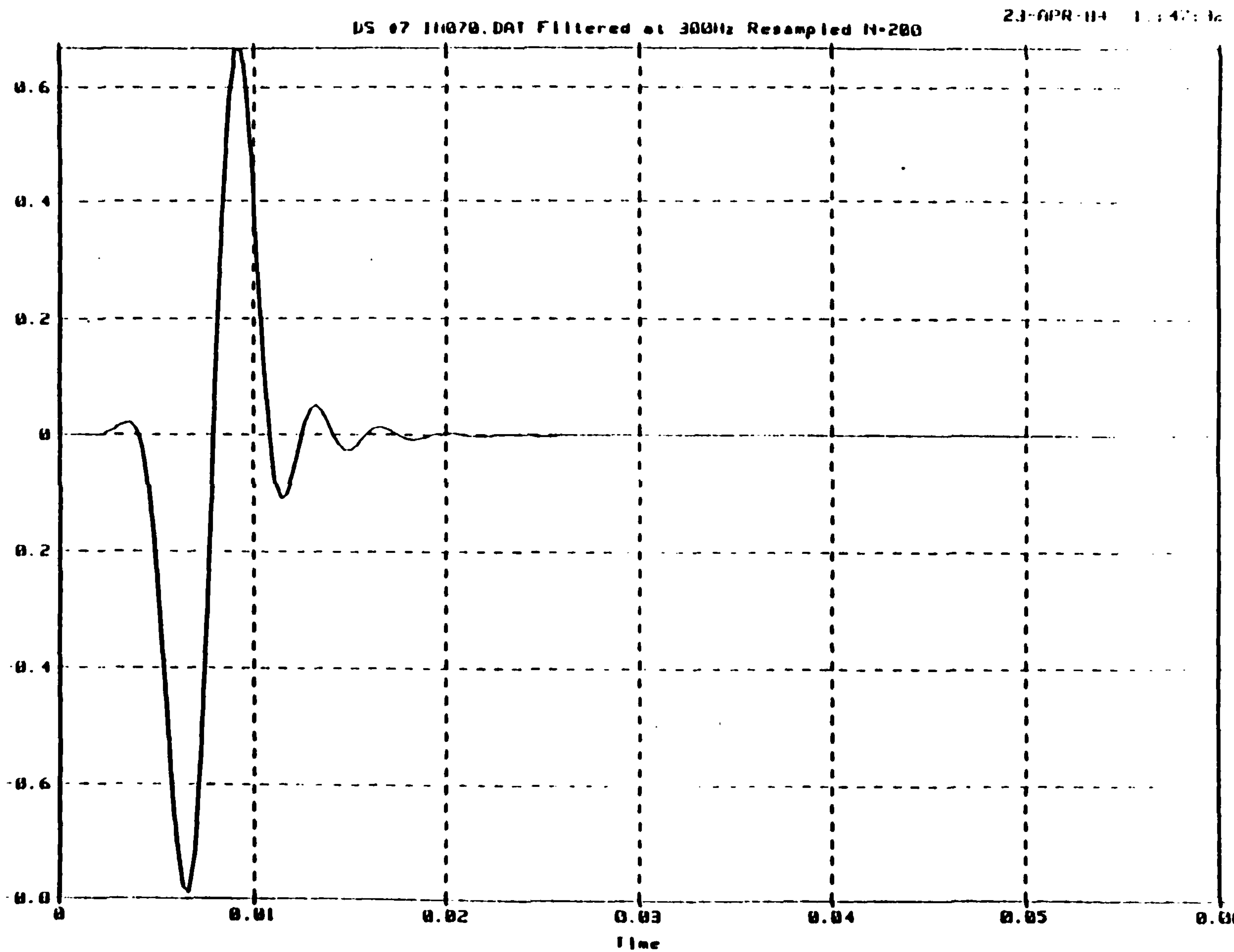

Fig. 5. Input signal, filtered at 300 hertz, decimated to 200 points.

sig

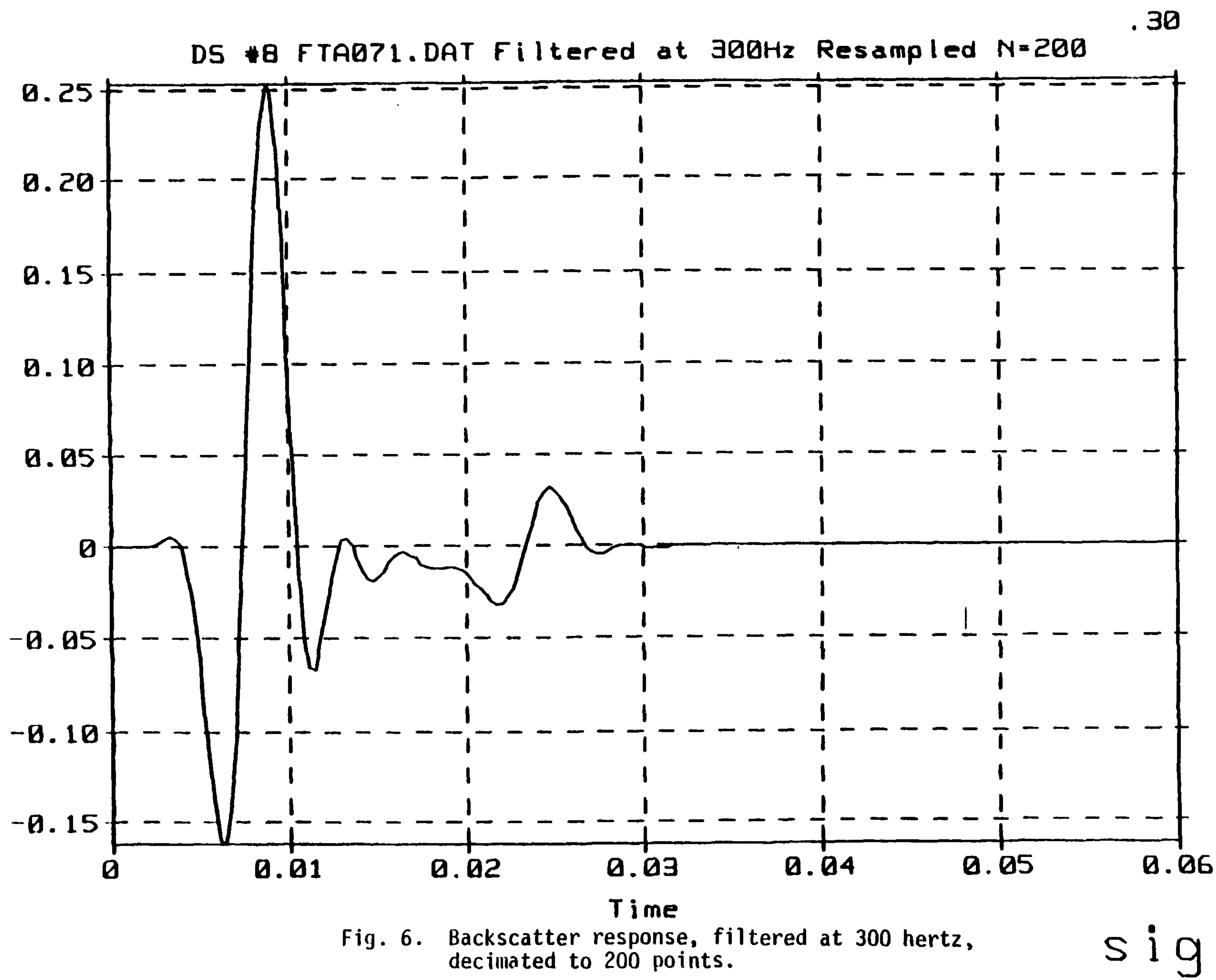

Fig. 6. Backscatter response, filtered at 300 hertz, decimated to 200 points.

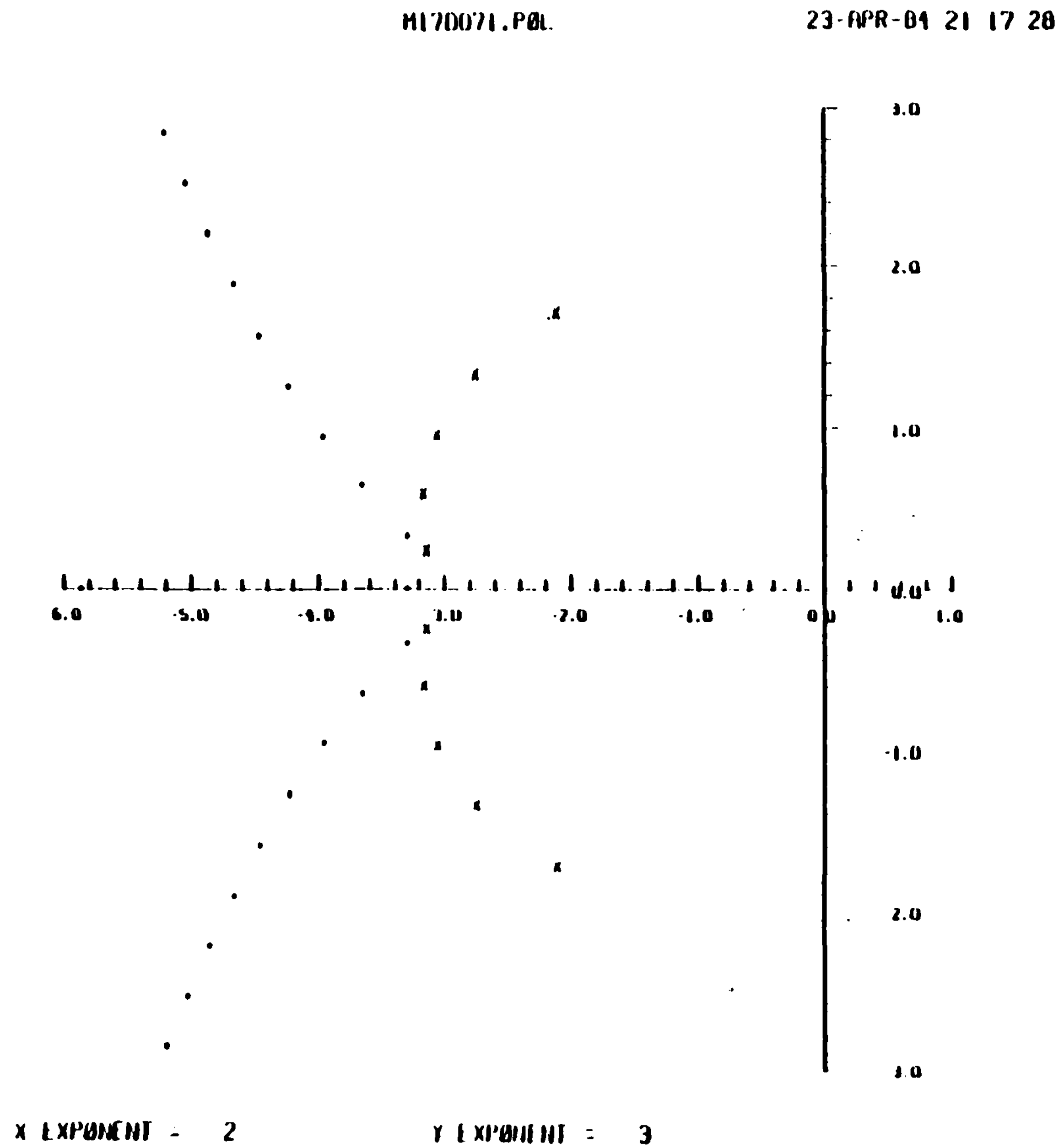

Fig. 7. Identified (x) and theoretical (+) poles, s-plane, 17th order model.

M40D071.P0L

4-MAY-84 07 35 02

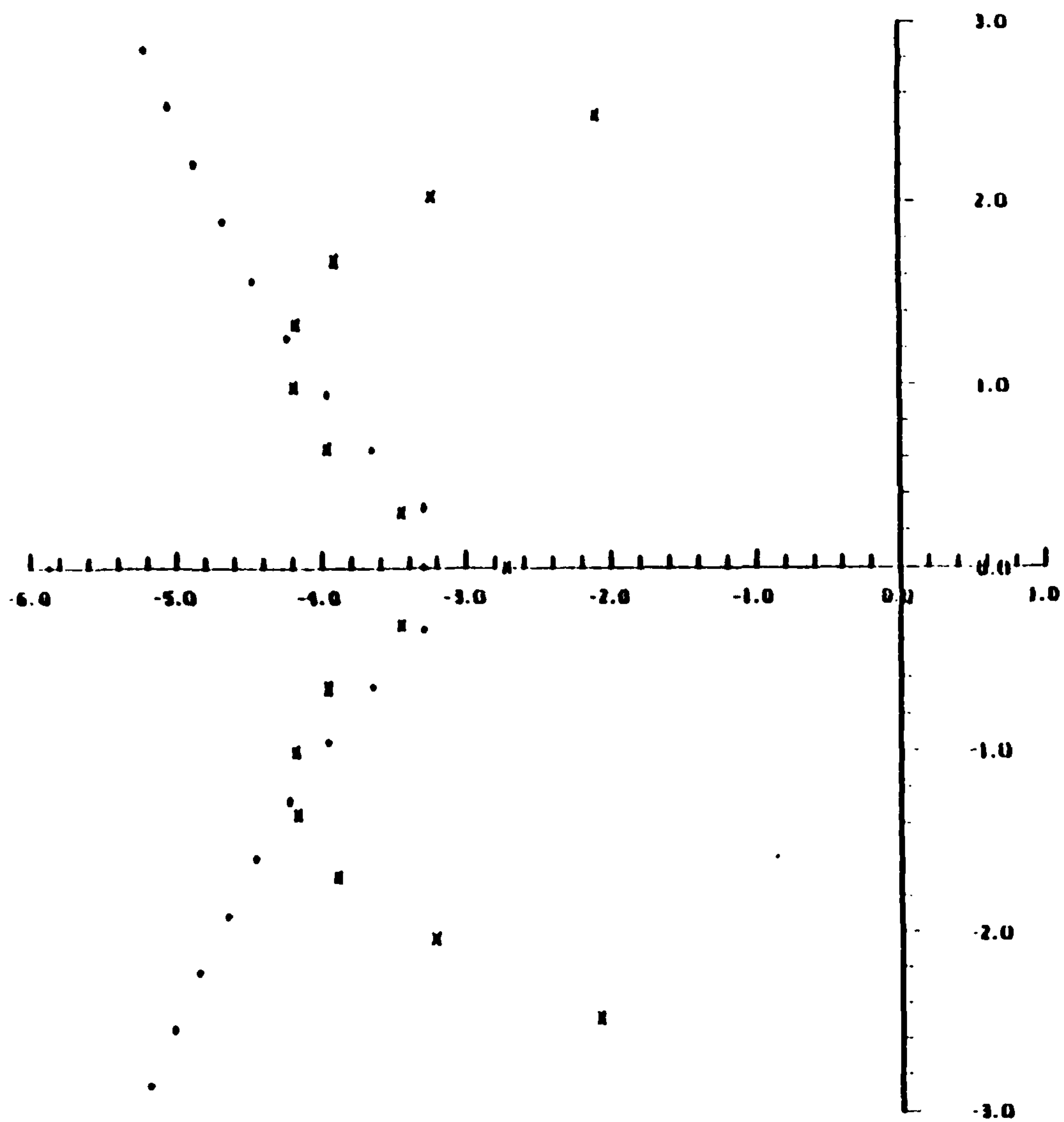

X EXPONENT = 2

Y EXPONENT = 3

Fig. 8. Identified (x) and theoretical (+) poles, s-plane, 40th order model.

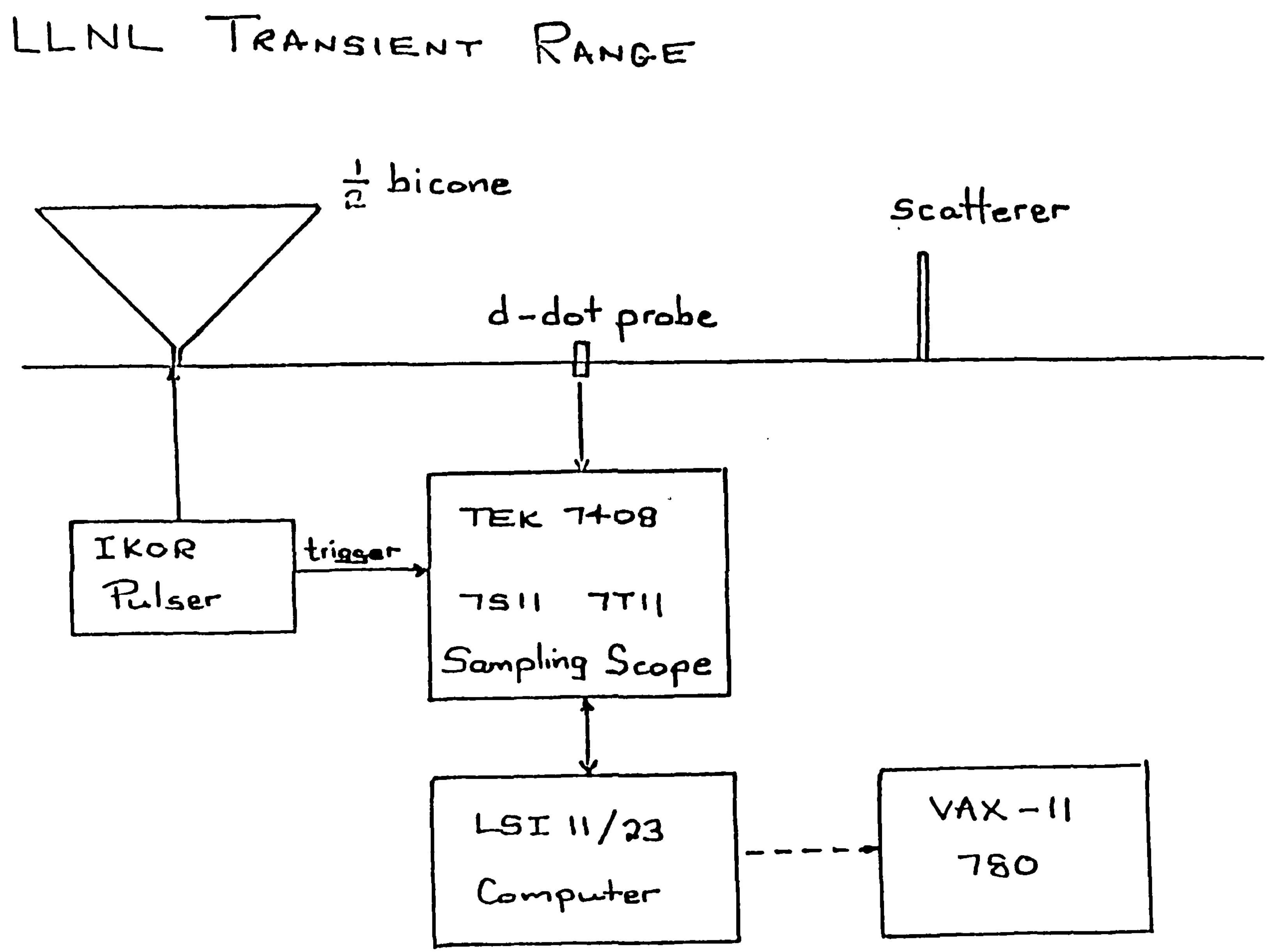

Fig. 9. Lawrence Livermore National Laboratory transient range.

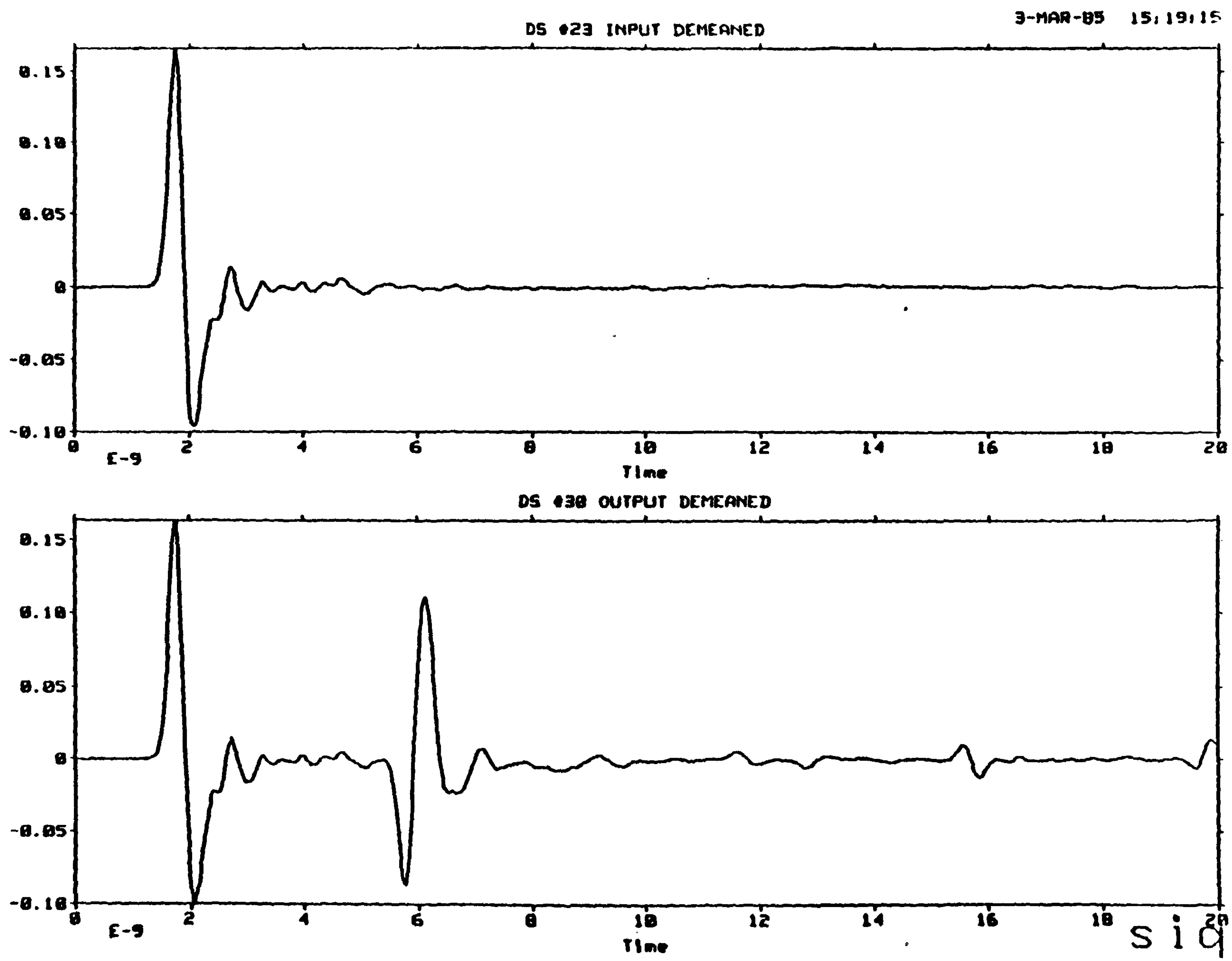

Fig. 10. Input and output, aluminum plate, 30 cm high by 60 cm wide; backscatter data, 2 feet from plate; 1024 points, 1.953×10^{-11} sampling rate; mean value removed.

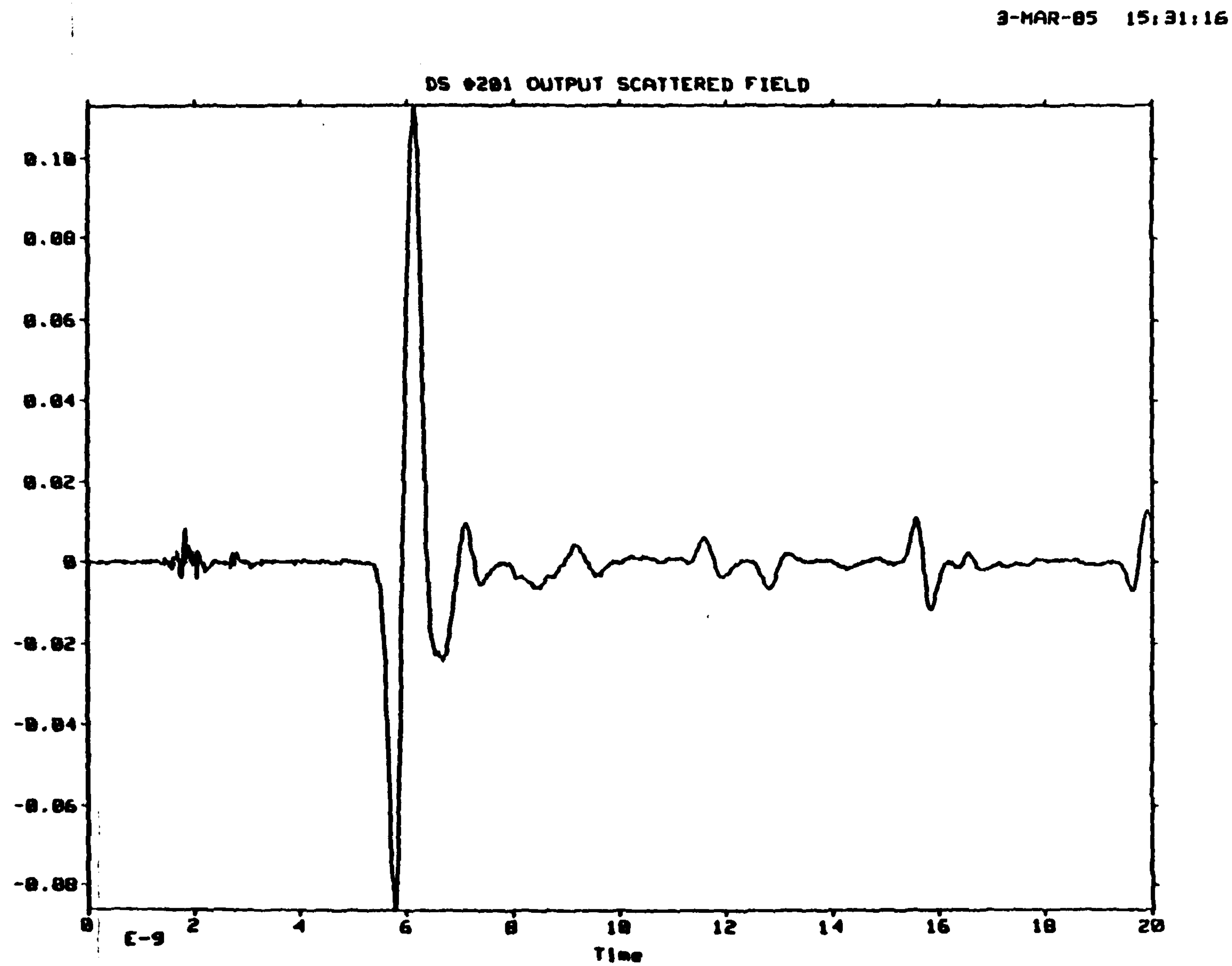

Fig. 11. Output with input subtracted (note precursor).

sig

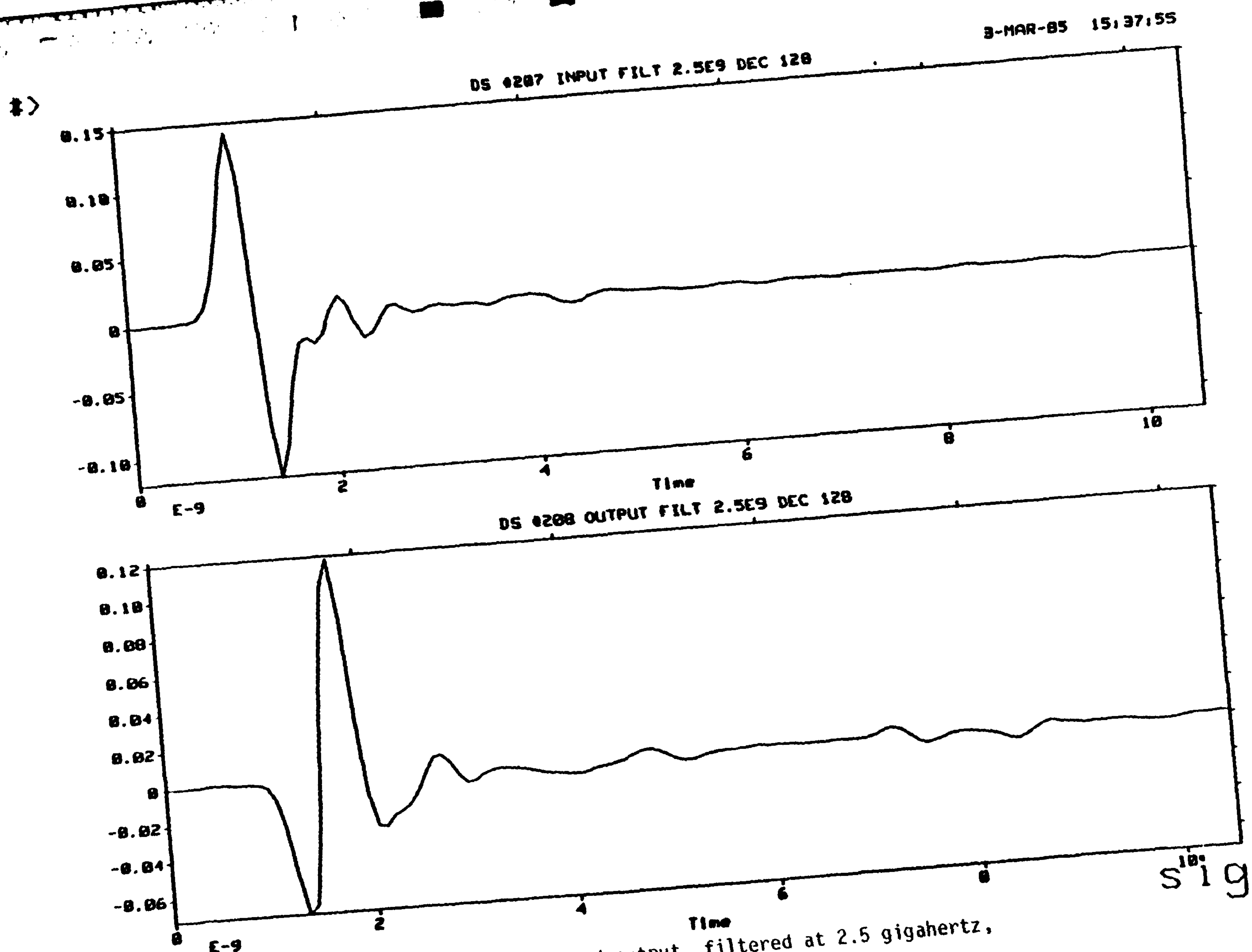

Fig. 12. Input and output, filtered at 2.5 gigahertz, decimated to 128 points.

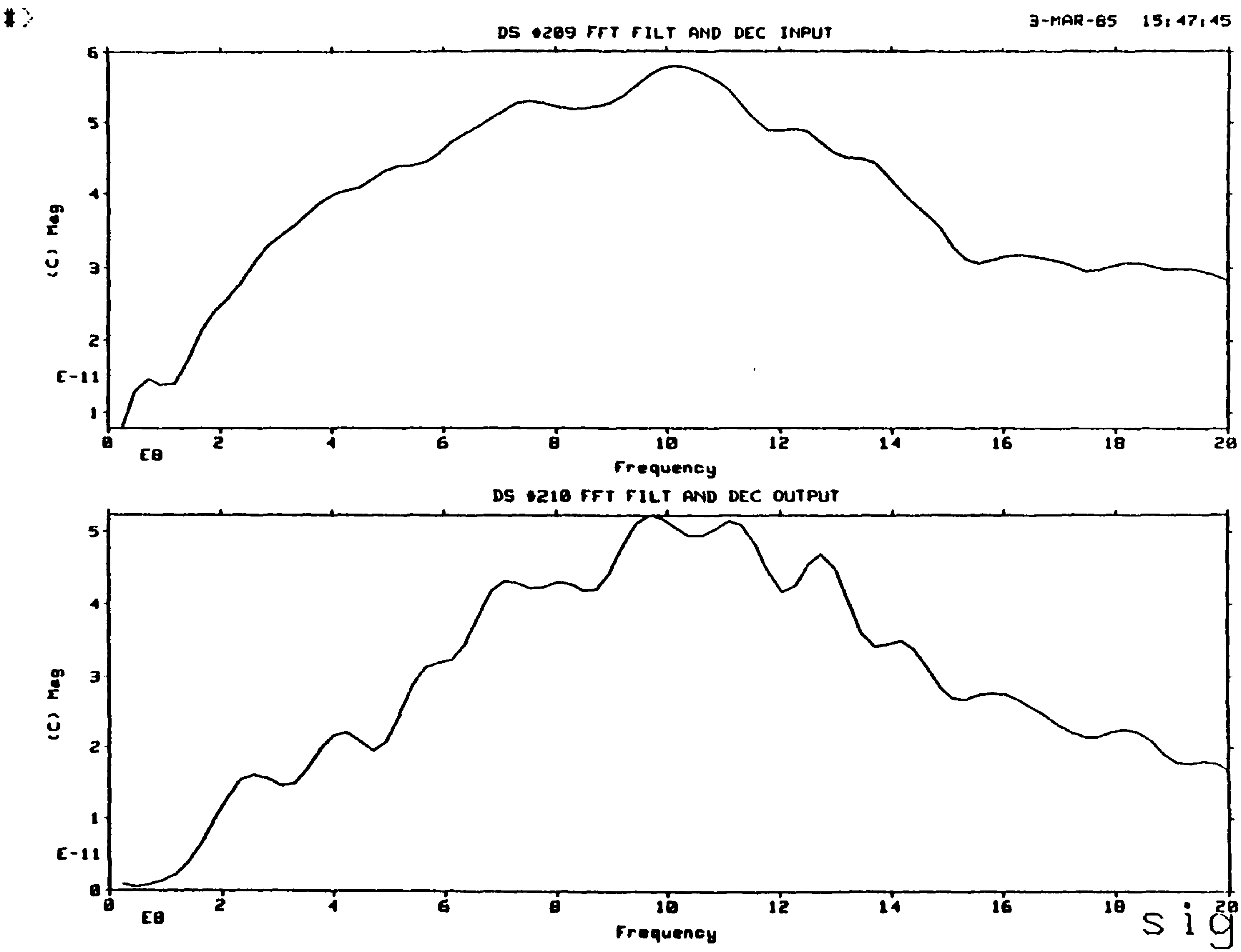

Fig. 13. FFT of filtered and decimated input and output.

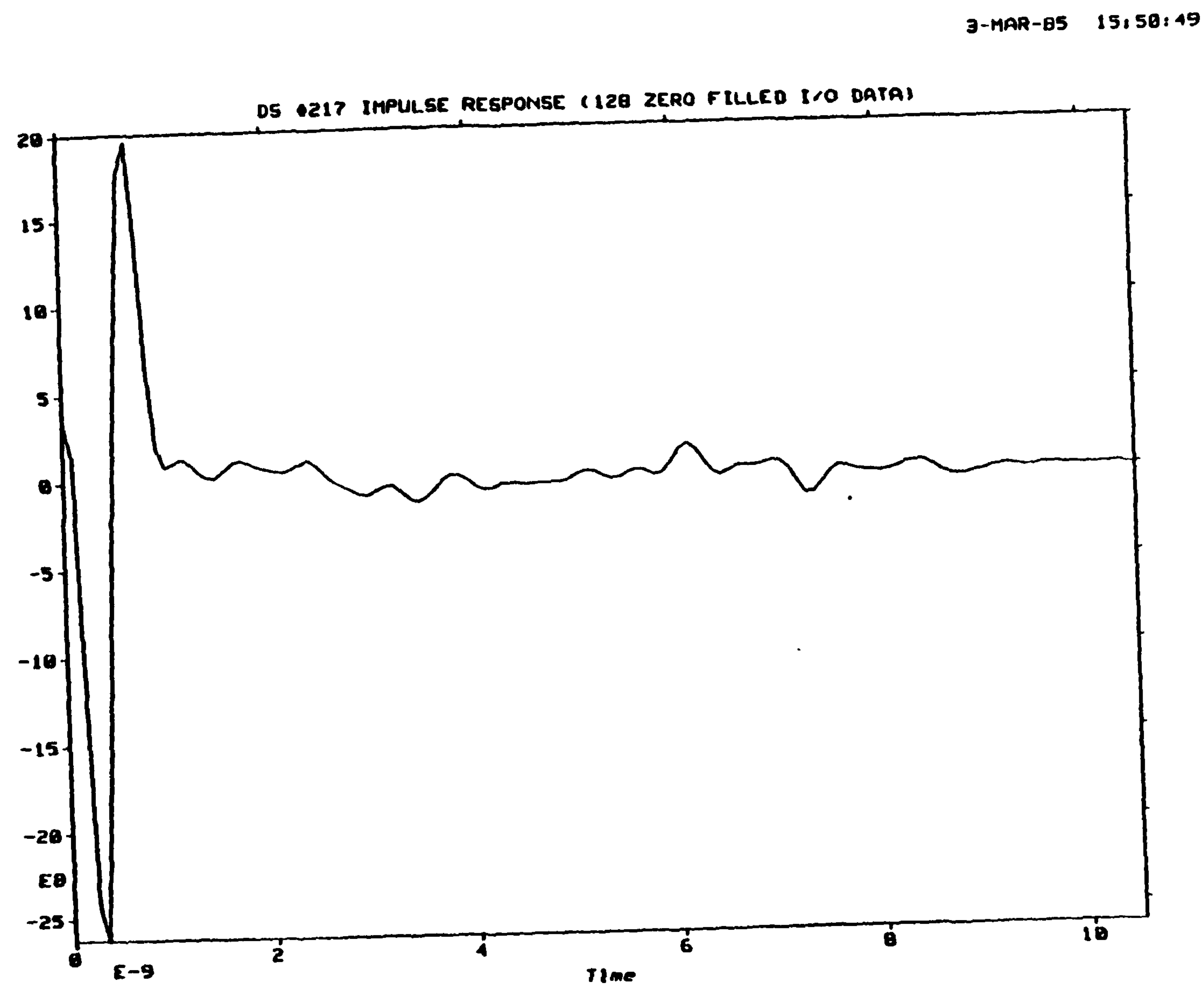

Fig. 14. Bandlimited impulse response (Weiner filter).

sig

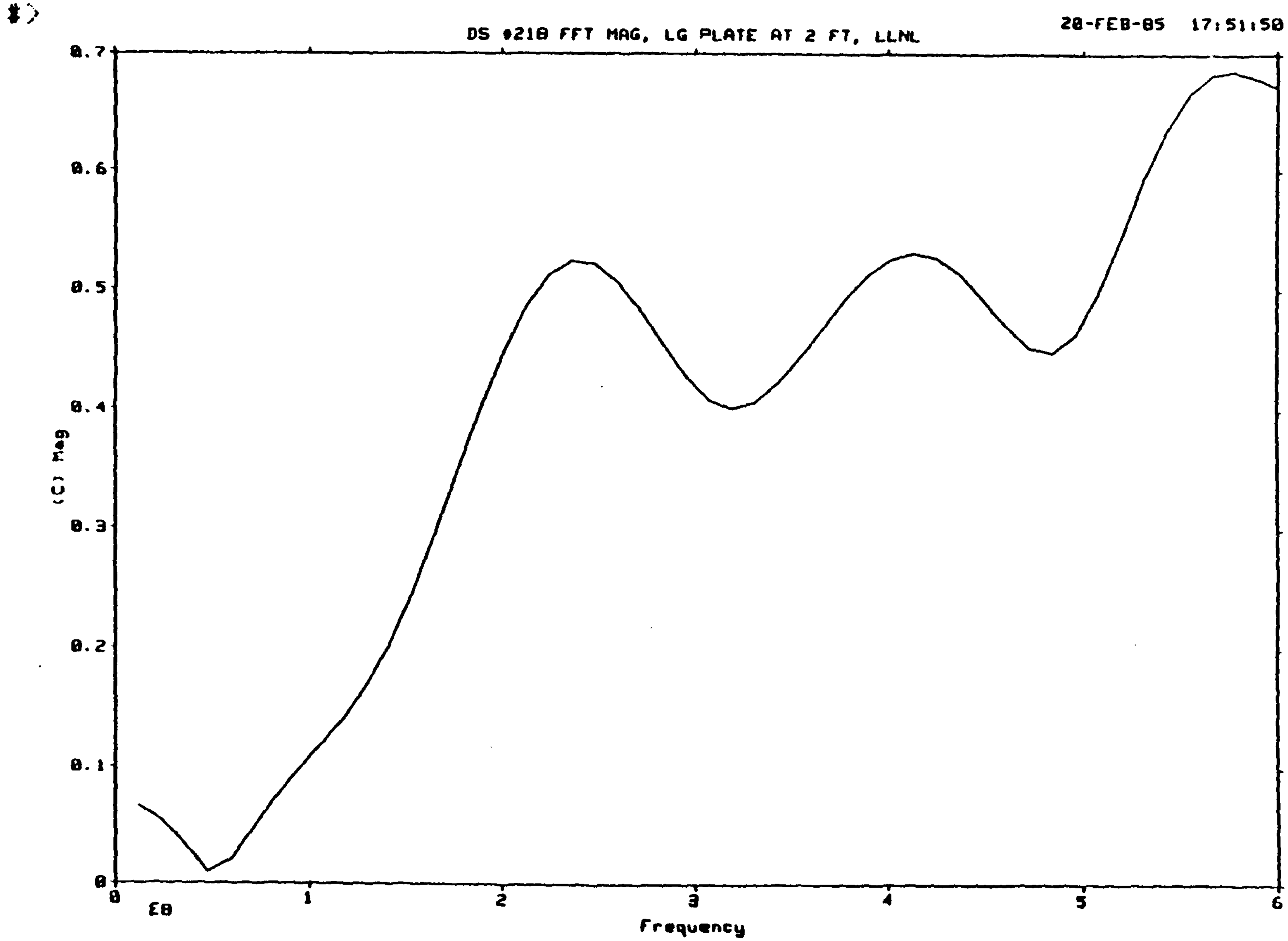

Fig. 15. FFT of impulse response.

sig

#>

3-MAR-85 16:02:24

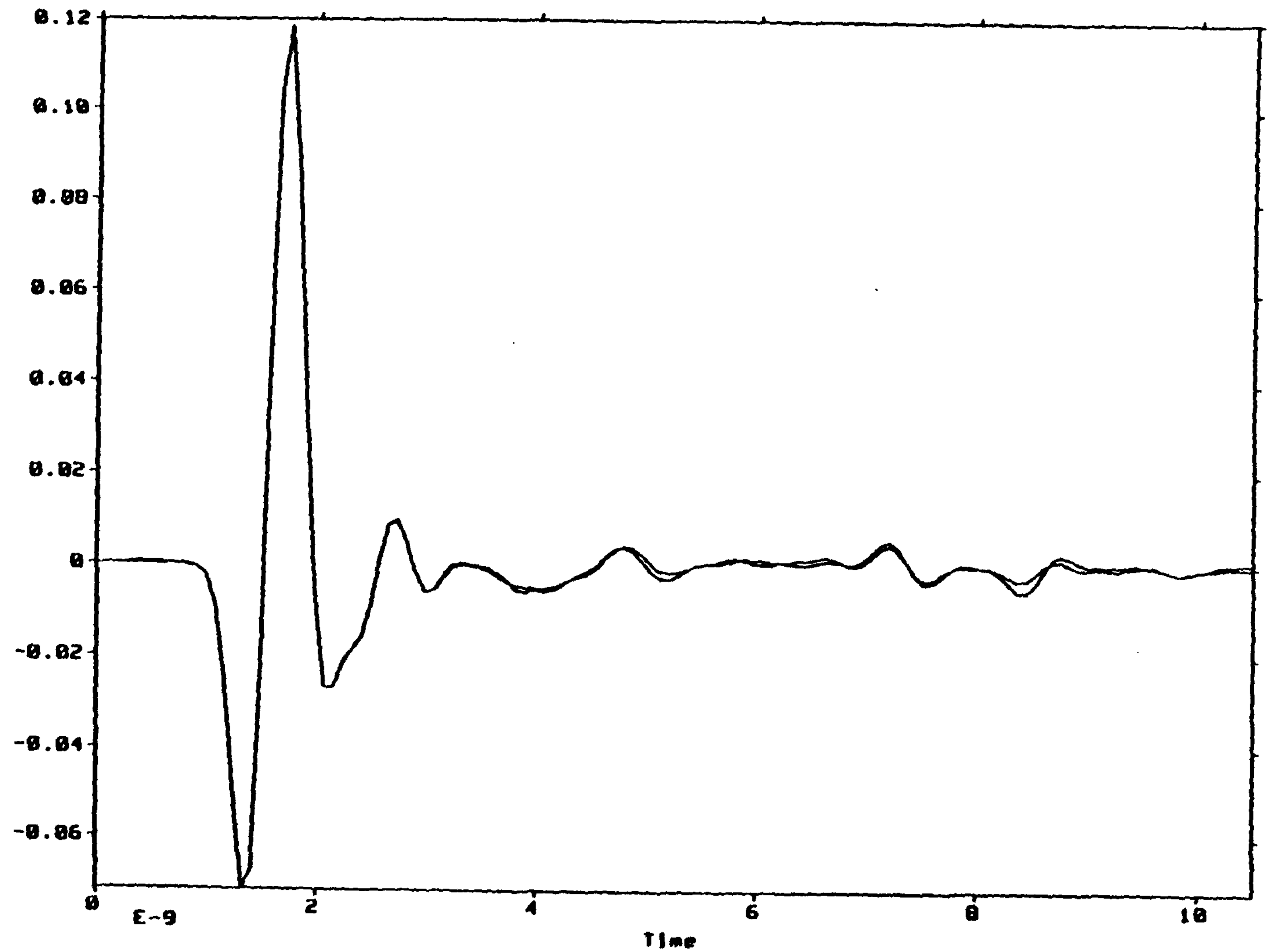

Fig. 16. Scattered field compared with 45th order model output from NLS.

sig

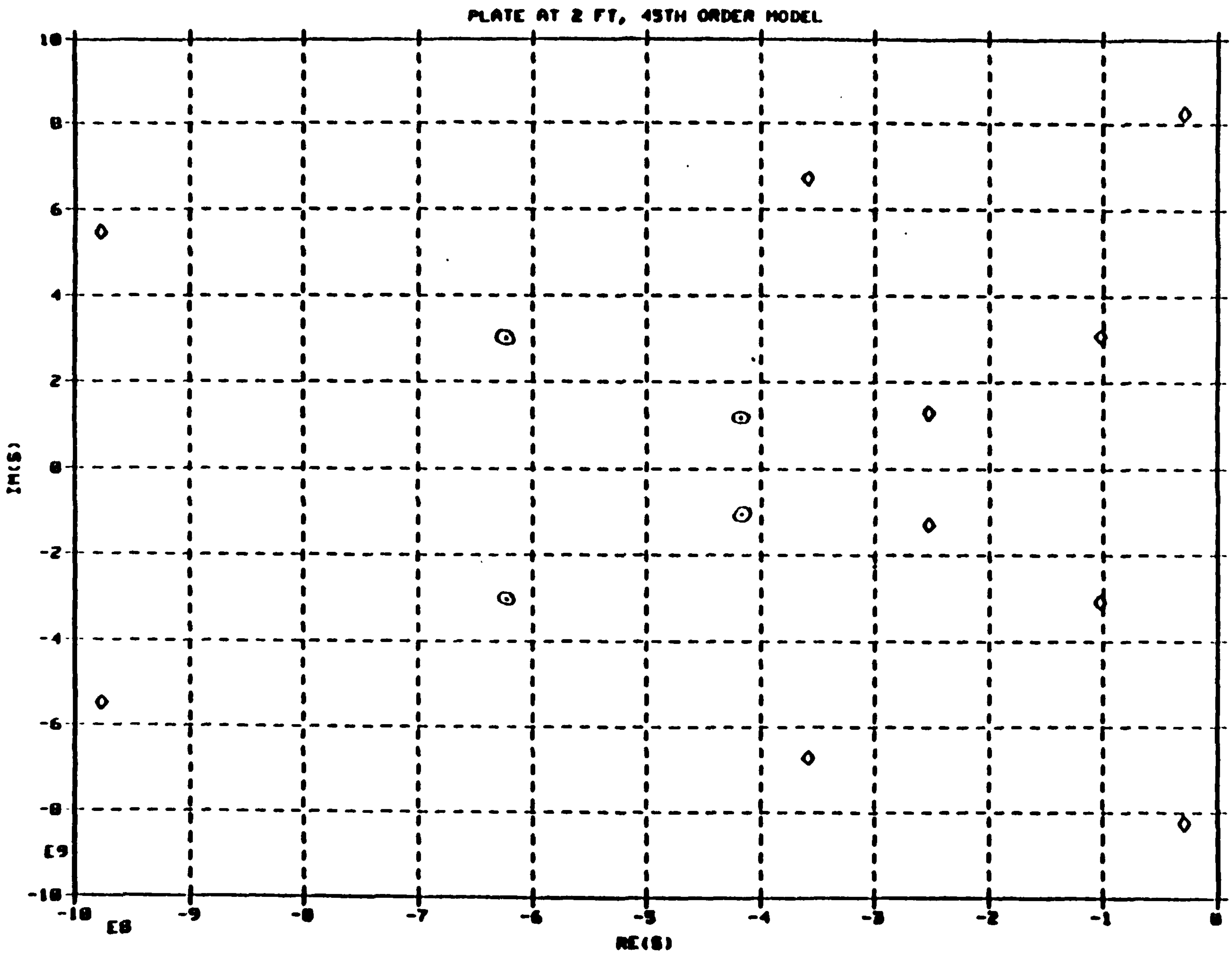

Fig. 17. Model poles (◊) compared with theoretical poles (⊙) (Pearson, 1976).

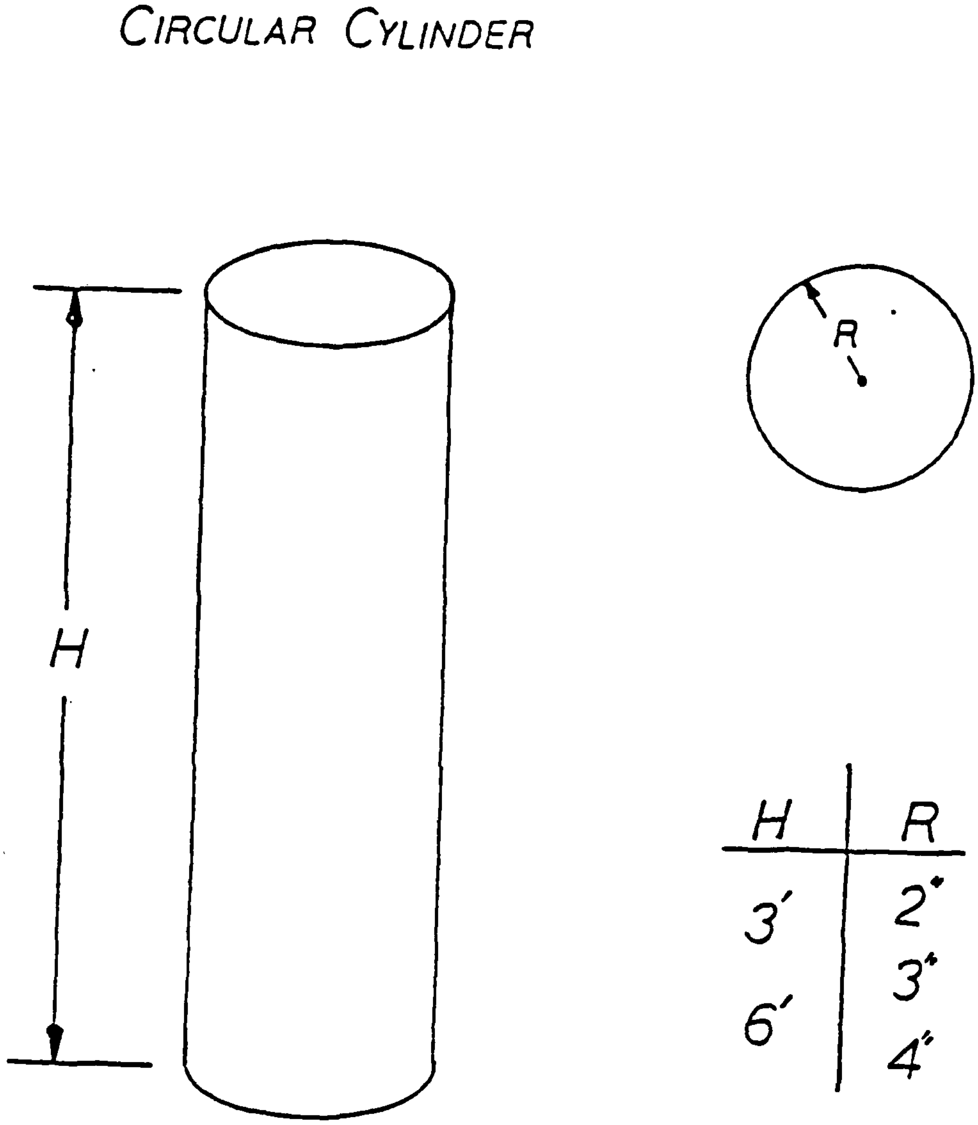

Fig. 18. Circular cylinder experimental models.

Parabolic Cylinder

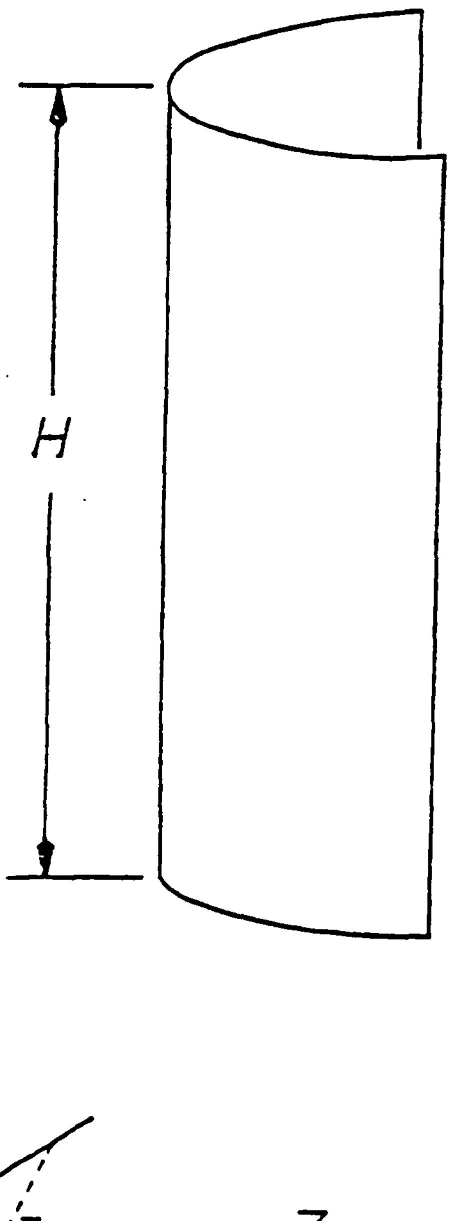

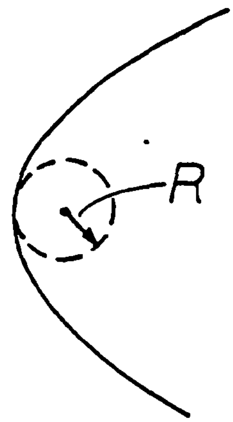

H	R
6′	2″
	4″

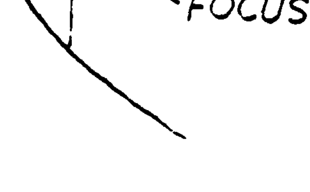

$$Z = \frac{P}{1 - \cos\theta}$$

NOTE: $R = \frac{P}{2}$

Fig. 19. Parabolic cylinder experimental models.

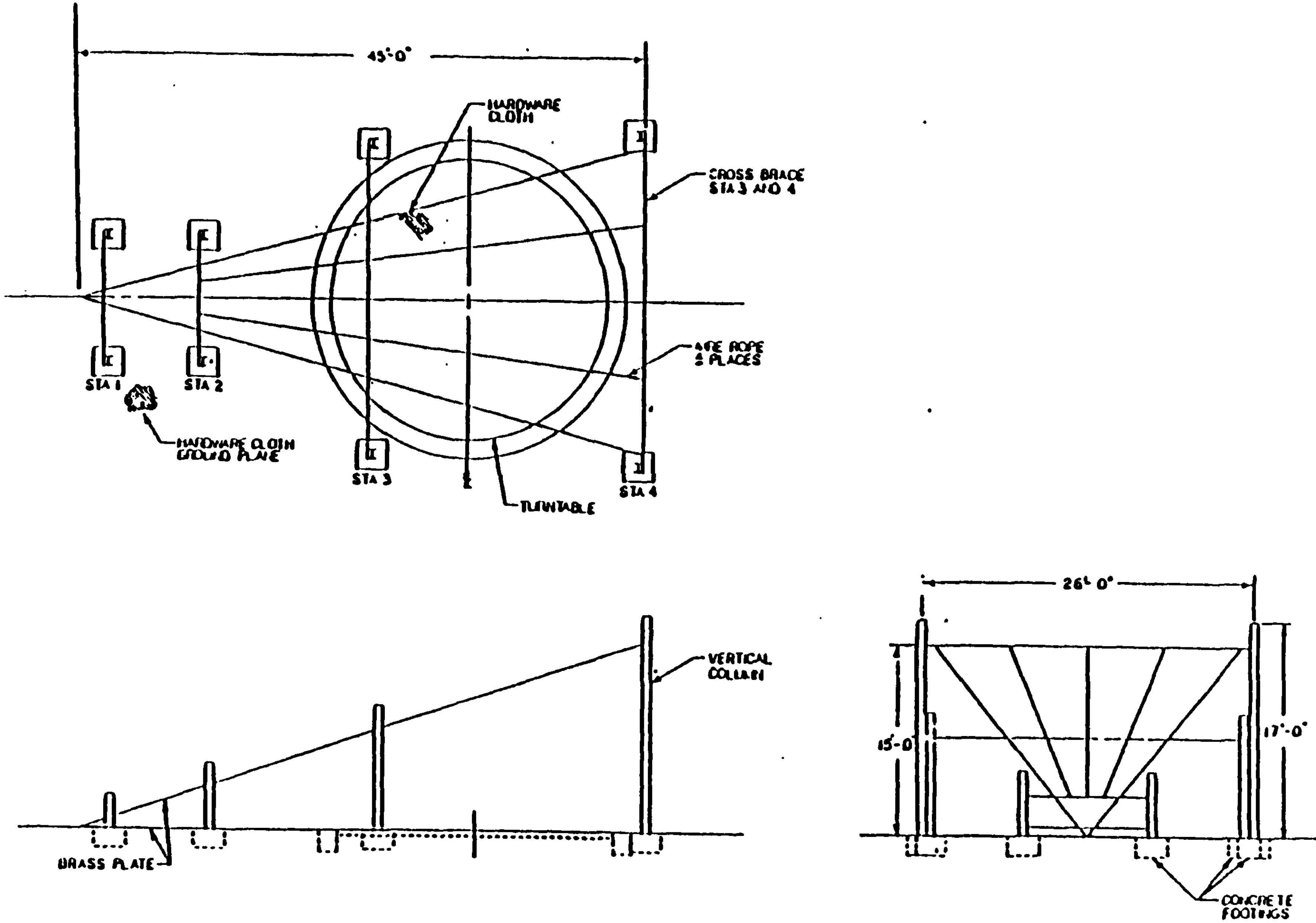

Fig. 20. NOSC transient range.

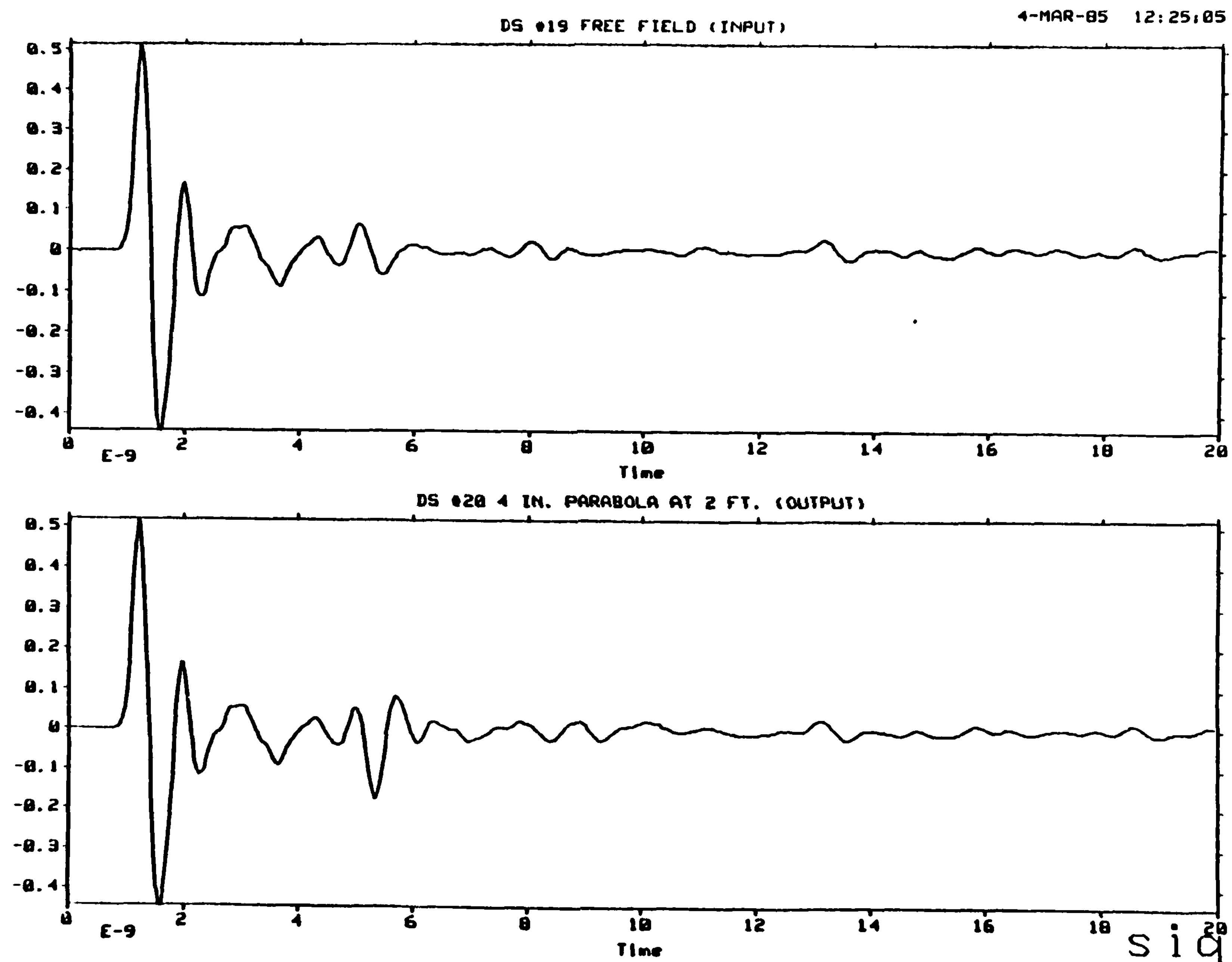

Fig. 21. Free field and total field, 4 inch parabola.

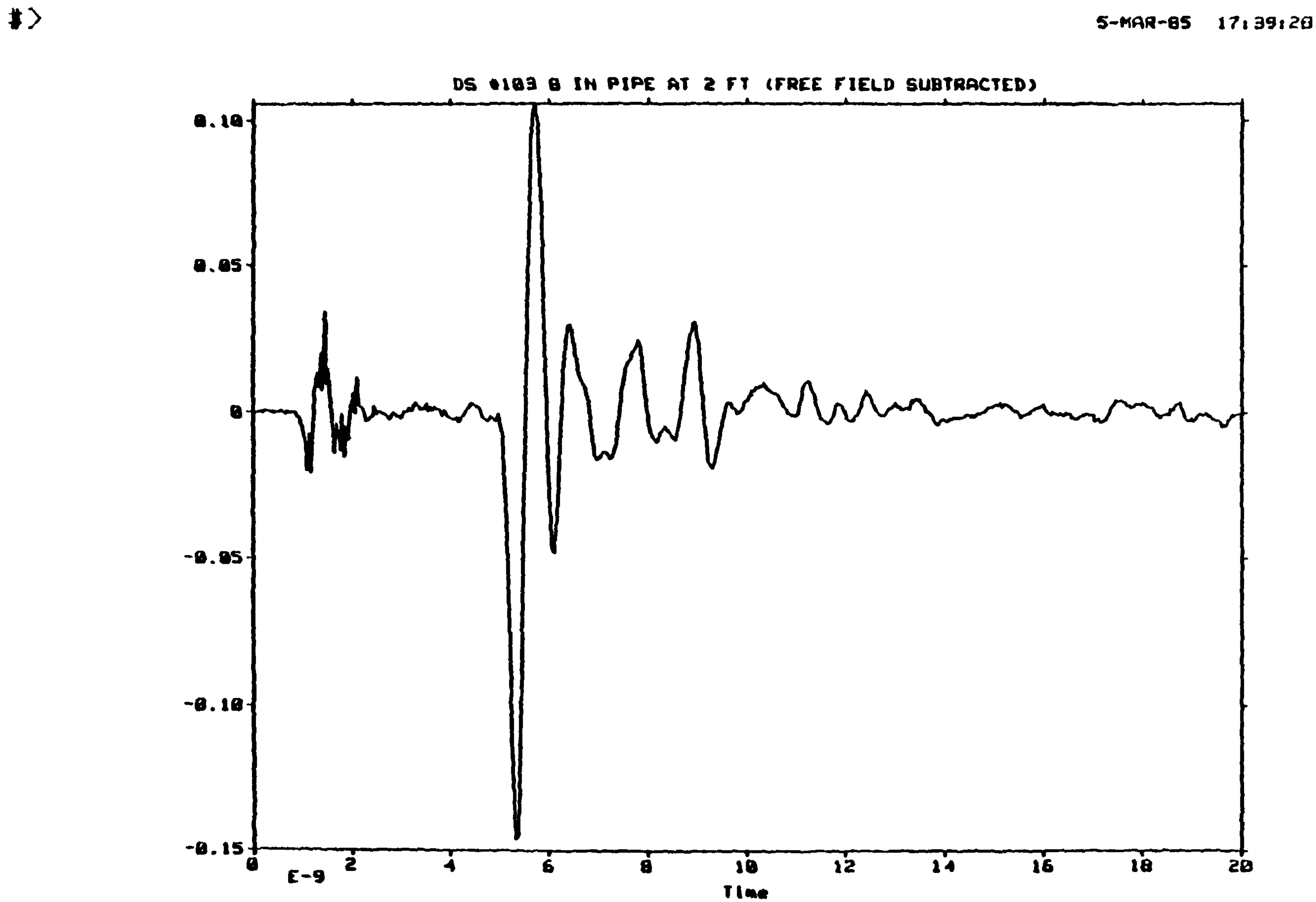

Fig. 22. Scattered field (note precursor).

sig

5-MAR-85 17:48:44

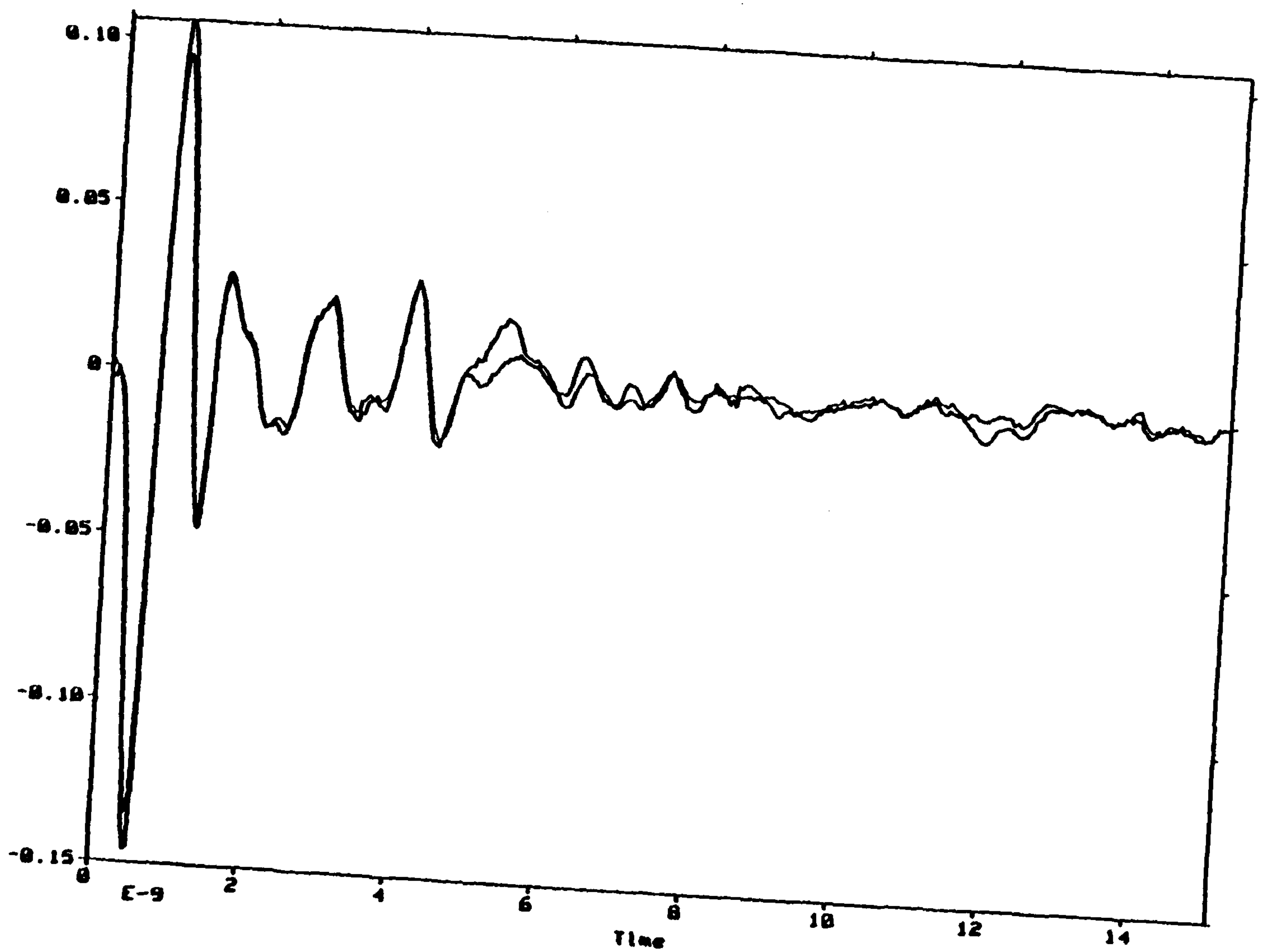

Fig. 23. Scattered fields from 4 inch parabola and 4 inch pipe.

sig

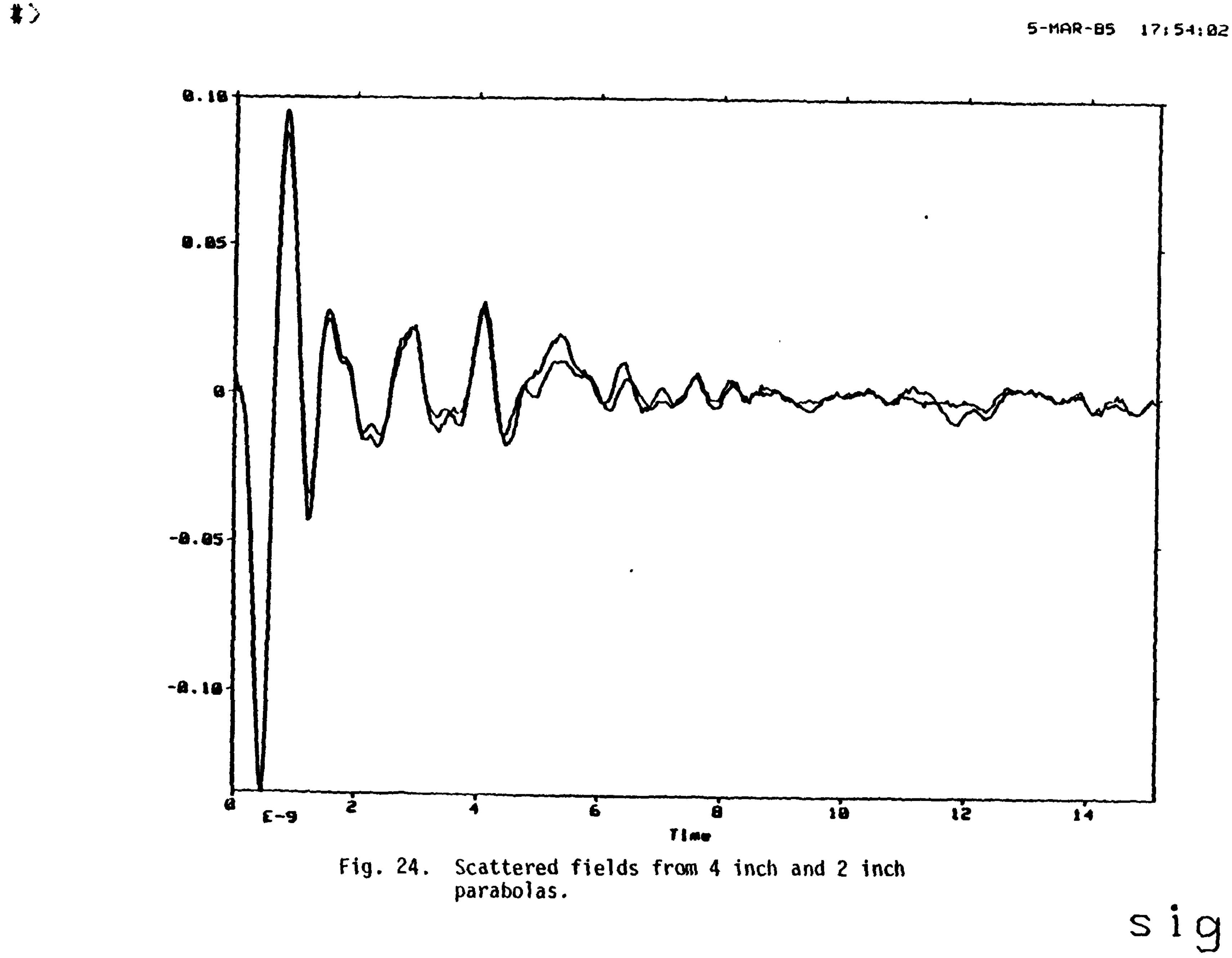

Fig. 24. Scattered fields from 4 inch and 2 inch parabolas.

5. REFERENCES

Bowman, J. J., T.B.A. Senior, and P.L.E. Uslenghi, Electromagnetic Scattering by Simple Shapes, North Holland.

Dudley, D. G. (1975), Numerical inversion of the Fourier transform: A combination trapazoidal and Filon technique, UCRL-51878, Lawrence Livermore National Laboratory, Livermore, CA 94550.

Dudley, D. G. (1979), Parametric modeling of transient electromagnetic systems, Radio Science 14, 387-396.

Dudley, D. G. (1983), Parametric identification of transient electromagnetic systems, Wave Motion 5, 369-384.

Dudley, D. G. (1984a), Electromagnetic target classification, Final Report, Contract N00019-82-C-0371, AIR330R, Naval Air Systems Command, Washington, DC 20361.

Dudley, D. G. (1984b), Global and local feature target classification, Quarterly Technical Report, Third Quarter, Contract N00019-83-C-0362, AIR330R, Naval Air Systems Command.

Dudley, D. G. (1985), Comments on SEM and the parametric inverse problem, IEEE Trans. Antennas and Propagation, 119-120.

Felsen, L. B. (1985), Comments on early time SEM, IEEE Trans. Antennas and Propagation, 118-119.

Goodman, D. M. (1983), NLS: A system identification package for transient signals, UCID-19767, Lawrence Livermore National Laboratory, Livermore CA 94550.

Marin, L. (1973), Natural-mode representation of transient scattered fields, IEEE Trans. Antennas and Propagation AP-21, 809-818.

Morgan, M. A. (1984), Singularity expansion representations of fields and currents in transient scattering, IEEE Trans. Antennas and Propagation AP-32, 466-473.

Pearson, L. W. (1976), The singularity expansion representation of the transient electromagnetic coupling through a rectangular aperture, Doctoral Dissertation, Department of Electrical Engineering, University of Illinois, Urbana-Champaign.

Pearson, L. W. (1984), A note on the representation of scattered fields as a singularity expansion, IEEE Trans. Antennas and Propagation AP-32, 520-524.

END

FILMED

6-85

DTIC